PAPER

Check for updates

Enhancing the stability of photocatalytic systems for hydrogen evolution in water by using a tris-phenyl-phenanthroline sulfonate ruthenium photosensitizer†

Fakourou Camara,[ab] Juan S. Aguirre-Araque,[a] Jérôme Fortage [ID] *[a] and Marie-Noëlle Collomb [ID] *[a]

The family of ruthenium tris-bipyridine complexes remains among the most widely used molecular photosensitizers (PSs) to drive catalytic reactions using the energy of light. However, the main drawback of such PSs is the poor stability of their oxidized and reduced forms subject to ligand dissociation, especially in water that causes relatively fast deactivation of the photocatalytic systems. We were able to improve the stability and efficiency of a Ru based photocatalytic system for hydrogen production in water by using the water-soluble $Na_4[Ru((SO_3Ph)_2phen)_3]$ derivative (**RuSPhphen**, $(SO_3Ph)_2phen$ = disodium (1,10-phenanthroline-4,7-diyl)bis(benzenesulfonate)) in place of regular $[Ru^{II}(bpy)_3]Cl_2$ (**Rubpy**, bpy = 2,2'-bipyridine) PS. **RuSPhphen** was tested with the $[Co^{III}(CR14)Cl_2]Cl$ (**Co**) catalyst and ascorbate (HA^-) as a sacrificial electron donor under visible-light irradiation. The **RuSPhphen** absorption coefficient being twice as high compared to **Rubpy** and the excited-state lifetime being much longer, while keeping almost similar potentials, more efficient intermolecular electron transfers have been observed allowing the concentration of Ru PSs to decrease by 5-fold, *i.e.* to 100 μM, compared to previous studies with the **Rubpy**/**Co**/HA^-/H_2A photocatalytic system. A substantially enhanced H_2-evolving photocatalytic activity was obtained with **RuSPhphen** directly correlated to its better stability over **Rubpy**. With 1.1 M H_2A/HA^-, at catalyst concentrations of 10 an 5 μM, the H_2 production is two times higher compared to that obtained with **Rubpy**. When the H_2A/HA^- concentration is decreased to 0.1 M, the stability of both Ru PSs is further improved although **RuSPhphen** still systematically outperforms **Rubpy** whatever the catalyst concentration, with TONs reaching up to 4770 at 5 μM catalyst. A faster electron transfer of the **RuSPhphen** excited state to HA^- has been observed by time-resolved luminescence compared to that of **Rubpy**, that could be ascribed to its much longer lifetime. In addition, a much higher rate constant for back electron transfer from the **RuSPhphen**·⁻ reduced state to $HA^•$ was determined by nanosecond transient absorption spectroscopy that could contribute to the higher stability of **RuSPhphen** during photocatalysis. The greater stability of **RuSPhphen** over **Rubpy** could also be correlated to the geometry of the SPhphen ligand that makes it less prone to dissociation in water in its reduced state.

Introduction
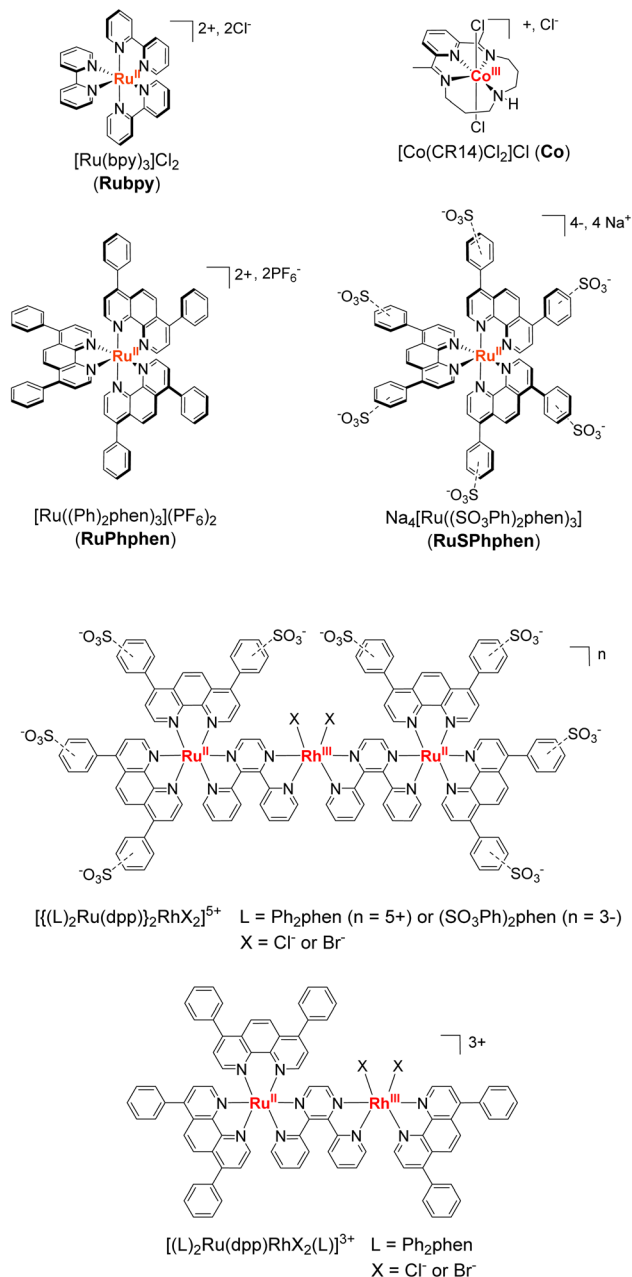
The unique spectroscopic, photophysical and electrochemical properties of ruthenium(II) complexes of the type $[Ru^{II}(L)]_3^{2+}$ with 2,2'-bipyridyl and 1,10-phenanthroline ligands and their

derivatives have made them extensively used for decades as molecular photosensitizers (PSs) for the activation of catalytic reactions using visible light energy.[1–9] Indeed, their long life-time in their triplet excited state, their intense absorption in the visible range, and their strong reducing and oxidizing power both in the excited and ground states as well as their solubility in water and organic solvents, make them very interesting PSs able to activate a wide range of catalysts for both oxidation and reduction reactions. Various reactions have been successfully carried out with such Ru derivatives, both in homogeneous solution and on surfaces (photoelectrodes), including the activation of organic substrates,[10–14] the oxidation of water to O_2 (oxygen-evolution-reaction (OER)),[15–18] the reduction of water (protons) to H_2 (hydrogen-evolution-reaction (HER))[19–22] and the

[a]Univ. Grenoble Alpes, CNRS, DCM, 38000 Grenoble, France. E-mail: jerome.fortage@univ-grenoble-alpes.fr; marie-noelle.collomb@univ-grenoble-alpes.fr

[b]Univ. Grenoble Alpes, CNRS, CEA, IRIG, SyMMES, 38000 Grenoble, France

† Electronic supplementary information (ESI) available: Materials, general experimental details, preparation and characterisation (¹H NMR, ESI-MS) of **RuSPhphen**, and additional data for electrochemistry, UV-visible absorption spectroscopy, photocatalytic hydrogen production, emission spectroscopy, Stern–Volmer plot and nanosecond transient absorption spectroscopy (Tables S1–S3 and Fig. S1–S10). See DOI: https://doi.org/10.1039/d3se01556d

reduction of CO_2.[23–30] However, besides the fact that they are based on rare and expensive metals, the main drawback of Ru derivatives is the instability of their reduced $[Ru^{II}(L)_2(L^{\bullet-})]^+$ and oxidized $[Ru^{III}(L)_3]^{3+}$ forms, that easily undergo a bidentate ligand substitution by solvent molecules or anions present in the medium, especially in aqueous solvent.[7,31–36] Molecular PSs based on Ir, Re and Pt noble metals have demonstrated good performances in photocatalysis for H_2 production or CO_2 reduction. However, Ir and Re PSs are generally limited by their poor absorption in the visible region, while Pt PSs commonly photobleach under prolonged irradiation.[37] Regarding organic dyes,[38,39] they are generally restrained by very short singlet excited state lifetimes and less negative reduction potentials than noble-metal based PSs, together with their fast photobleaching.[40]

In this context, given the quite unique properties of Ru complexes as PSs, progress should be made to increase their stability. Among the existing Ru derivatives, the tris-diphenyl-phenanthroline complex, $[Ru(Ph_2phen)_3]^{2+}$ (Ph_2phen = 4,7-diphenyl-1,10-phenanthroline or bathophenanthroline) (denoted as **RuPhphen**),[2] and the water-soluble sulfonate analog $Na_4[Ru((SO_3Ph)_2phen)_3]$ (($SO_3Ph)_2phen$ = disodium (1,10-phenanthroline-4,7-diyl)bis(benzenesulfonate)) (denoted as **RuSPhphen**)[41] (Scheme 1) have particularly retained our attention. In fact, such PSs exhibit absorption coefficients twice as high compared to regular $[Ru(bpy)_3]^{2+}$ (bpy = 2,2'-bipyridine) (denoted as **Rubpy**) and much longer lifetime of their excited-state, while keeping almost similar potentials. In addition, the group of Castellano[42] has shown that **RuPhphen** is more stable than **Rubpy** allowing enhanced H_2 production when used in a homogeneous photocatalytic system with a cobalt glyoxime catalyst (Cat), $[Co(dmgH)_2pyCl]$ (dmgH = dimethylglyoxime, py = pyridine) and N,N'-dimethyl-p-toluidine (DMT) as a sacrificial electron donor (SD) in a CH_3CN/H_2O mixture (1 : 1). It has been proposed that the better stability of the photocatalytic system with **RuPhphen** over **Rubpy** may result from the higher rigidity of the **RuPhphen** complex induced by the large diphenyl-phenanthroline ligand, which makes it less prone to ligand loss/substitution. In addition, a high rate constant for reductive quenching between the excited state of **RuPhphen** and DMT was reported which was attributed to the long lifetime of the PS's excited state (5.86 μs) that facilitates bimolecular electron-transfer reactions.[42] The group of Brewer also reported substantially enhanced H_2-evolving photocatalytic activity with supramolecular RuRh photocatalysts of the triad and diad type through the use of diphenyl-phenanthroline terminal ligands on the Ru moieties in place of regular phen or bpy ligands (Scheme 1).[43–48] Since the observed excited state rate constants do not vary greatly, the steric protection of the Rh catalyst by the bulkier terminal ligand was suggested as a possible factor in the enhanced catalytic performances, decreasing unfavorable side reactions such as dimerization of the Rh catalytic site in the case of the RuRh diad. In addition, it has been proposed that the larger size of the diphenyl-phenanthroline ligand may provide for a lower rate of back electron transfer to the photo-oxidized N,N-dimethylaniline (DMA) donor. Finally, the same group found that insertion of a hydrophilic sulfonate

Scheme 1 Ruthenium photosensitizers and cobalt catalysts studied in this work and ruthenium–rhodium photocatalysts of the triad and diad type developed by the group of Brewer.[43–49]

substituent on the phenyl units[49] increase the quantum yield of emission and the lifetime of the ^{3}MLCT excited state[20] and led to a water soluble H_2-evolution photocatalyst (Scheme 1). These interesting results prompt us to investigate the water-soluble **RuSPhphen** in a three-component photocatalytic system for H_2 production in fully aqueous solution.

In this contribution, we have tested the performance as a PS of the water-soluble **RuSPhphen** PS in association with one of the most efficient H_2-evolving catalysts in acidic water,[40,50–53] the cobalt tetraazamacrocyclic complex, $[Co^{III}(CR14)Cl_2]^+$ (denoted, **Co**) (CR14 = 2,12-dimethyl-3,7,11,17-tetraazabicyclo[11.3.1] heptadeca-1(17),2,11,13,15-pentaene) and ascorbate (HA^-) as
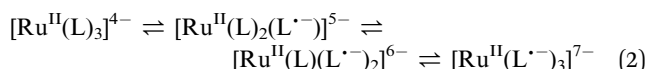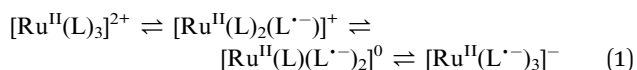
a SD (Scheme 1) under visible-light irradiation. We also performed comparative studies under similar conditions to the regular **Rubpy** PS. Various PSs and catalyst concentrations were investigated in two different aqueous media: 1.1 M HA_2/HA^- at pH 4.0 and 0.1 M HA_2/HA^- at pH 4.5 with 1 M acetate buffer. A substantially enhanced H_2-evolving photocatalytic activity was observed in both media with **RuSPhphen** compared to benchmark **Rubpy**, especially for lower catalyst concentrations, directly correlated to the better stability of **RuSPhphen** over **Rubpy**.

We have also investigated the redox properties of **RuSPhphen** in DMF to determine the stability of the reduced states of **RuSPhphen** and their UV-visible absorption signature. Finally, time-resolved luminescence and nanosecond transient absorption spectroscopy were employed to investigate the photocatalytic mechanism owing to the detection of key intermediates such as the excited and reduced states of the Ru PS as well as the reduced state of the catalyst (Co^I). The extracted kinetics parameters of the two PSs were compared in an effort to rationalize the greater stability of **RuSPhphen**.

Results and discussion

Electrochemical properties of RuSPhphen: generation and UV-visible characterization of the reduced states

The redox properties of **RuSPhphen** have been investigated in a degassed solution of DMF, 0.1 M $[Bu_4N](ClO_4)$ and compared to those of **Rubpy** under the same conditions. The cyclic voltammograms are characteristic of such derivatives[2,41] with a one-electron reversible metal-centered oxidation process (Ru^{III}/Ru^{II}) and three reversible ligand-centered reduction processes (eqn (1) for L = bpy and eqn (2) for L = $(SO_3Ph)_2phen$) (Fig. 1(A)). Potentials are quite similar for both complexes (Table S1†). For **RuSPhphen**, the reversible Ru^{III}/Ru^{II} oxidation system is located at +0.80 V *vs.* $Ag/AgNO_3$ (with this reference, the reversible ferrocene/ferrocenium redox couple was measured at $E_{1/2} = 60$ mV) and the three reversible ligand-centered reduction processes at $E_{1/2} = -1.61$, -1.78 and -2.00 V (Fig. 1). For **Rubpy**, the corresponding systems are observed at +0.88, -1.65, -1.82 and -2.09 V. The reducing power of **RuSPhphen** is thus nearly similar to that of **Rubpy** in organic solvent, with the first reduction process of **RuSPhphen** ($L/L^{•-}$) being less negative than that of **Rubpy** by 40 mV.

$$[Ru^{II}(L)_3]^{2+} \rightleftharpoons [Ru^{II}(L)_2(L^{•-})]^+ \rightleftharpoons$$
$$[Ru^{II}(L)(L^{•-})_2]^0 \rightleftharpoons [Ru^{II}(L^{•-})_3]^- \quad (1)$$

$$[Ru^{II}(L)_3]^{4-} \rightleftharpoons [Ru^{II}(L)_2(L^{•-})]^{5-} \rightleftharpoons$$
$$[Ru^{II}(L)(L^{•-})_2]^{6-} \rightleftharpoons [Ru^{II}(L^{•-})_3]^{7-} \quad (2)$$

To evaluate the stability in DMF of the **RuSPhphen** reduced species with the respective charges 5^-, 6^- and 7^- (eqn (2)) and assess their UV-vis signature, three successive electrolyses at -1.72, -1.90 and -2.20 V have been performed. The knowledge of the spectroscopic signature of the one electron reduced species of **RuSPhphen** (denoted as **RuSPhphen**$^{•-}$) will allow this
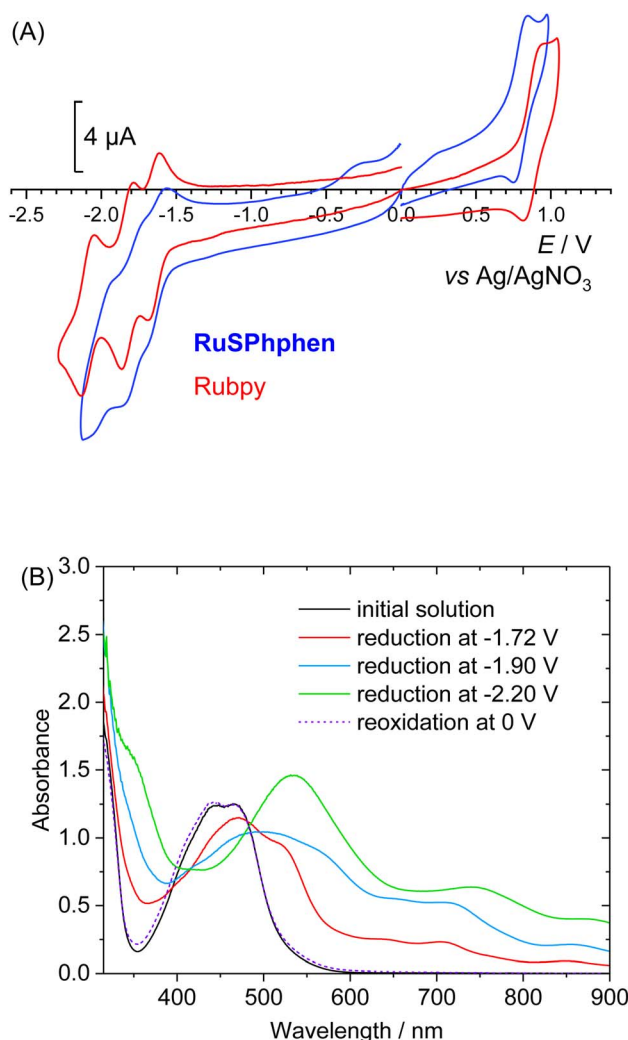
Fig. 1 (A) Cyclic voltammograms in DMF, 0.1 M $[Bu_4N]ClO_4$ at a glassy carbon electrode ($\varnothing = 3$ mm, $\nu = 100$ mV s^{-1}) of solutions of **RuSPhphen** (0.44 mM, blue line) and **Rubpy** (0.3 mM, red line). (B) UV-visible absorption spectral changes of the solution of **RuSPhphen** (0.44 mM) in DMF, 0.1 M $[Bu_4N]ClO_4$, after three successive exhaustive reductions at (a) $E = -1.72$ V (formation of **RuSPhphen**$^{5-}$ also denoted as **RuSPhphen**$^{•-}$), (b) -1.90 V (formation of **RuSPhphen**$^{6-}$), and (c) -2.20 V (formation of **RuSPhphen**$^{7-}$) and (d) after a reoxidation at 0.0 V (reformation of **RuSPhphen**). The optical path is 1 mm.

species to be easily identified by transient absorption spectroscopy and thus to ascertain the reductive quenching mechanism (see below).

Fig. 1(B) displays the UV-visible spectra of the initial solution and of the stepwise reduction species. As for **Rubpy**,[54] the spectra show the progressive decrease in intensity of the initial MLCT bands at 445 and 466 nm upon reduction, along with the corresponding increase of new bands progressively shifted at lower energy. An isobestic point is also observed at 485 nm. The maxima of these bands after the third reduction corresponding to the fully reduced species $[Ru^{II}(L^{•-})_3]^{7-}$ are located at 355 (sh), 553, 773 (sh) and 870 nm. The reduced solutions are perfectly stable showing the excellent stability of the three reduced states of the complex in organic solvent. A similar stability for the

three reduced states of **Rubpy** is obtained in DMF, with the resulting spectra being similar to those previously obtained in CH$_3$CN (Fig. S3†).[54] So, from this experiment in organic solvent, it is not possible to conclude the better stability of the one-electron reduced state of **RuSPhphen** to explain the higher stability of the photocatalytic system with this PS (see below). All reduction steps were found to be reversible as further reoxidation of the solution at a potential of 0 V fully restores the initial solution for both **RuSPhphen** and **Rubpy** (Fig. 1(B) and S3†).

Photocatalytic activities for hydrogen production with the RuSPhphen and Rubpy/Co/HA⁻/H$_2$A systems

Our previous studies with the **Rubpy**/[Co^{III}(CR14)Cl$_2$]$^+$ (**Co**)/HA⁻/H$_2$A system for photo-induced H$_2$ production were conducted in deaerated aqueous media under visible light irradiation (400–700 nm) with **Rubpy** at a concentration of 500 μM and various concentrations of **Co** catalyst, between 100 and 1 μM in the 1.1 M HA⁻/H$_2$A buffer[50,51,53] and between 50 and 5 μM in 1 M acetate buffer with 0.1 M of HA⁻/H$_2$A.[40] The best activities for H$_2$ production in these media were obtained at pH 4.0 and 4.5, respectively. The visible absorption (29 300 M⁻¹ cm⁻¹ at 462 nm) of **RuSPhphen** in water[41] is twice as high as that of the reference PS **Rubpy** (14 600 M⁻¹ cm⁻¹ at 452 nm) and the excited state lifetime of **RuSPhphen** (3.8 μs) is much longer than that of **Rubpy** (0.61 μs) in water (Table S2†). Electron transfers between the PS excited state and the SD and Cat should thus be favored and the photo-induced H$_2$ production is more efficient even at lower PS concentrations. We therefore decrease the concentration of **RuSPhphen** by 5-fold compared to previous studies, i.e. to 100 μM. Comparative experiments with the **Rubpy**/Co/HA⁻/H$_2$A system at a **Rubpy** concentration of 100 μM were also performed under the same experimental conditions for a more reliable comparison of the performance of the two PSs. Table S3† summarizes the photocatalytic activities of all studied systems.

The photocatalytic performances were first investigated in 1.1 M H$_2$A/HA⁻ at pH 4.0 with 100, 50, 10 and 5 μM of **Co** catalyst. Fig. 2 displays the comparison of both PSs activities as a function of time in terms of turnover number vs. catalyst (TON$_{Cat}$). The corresponding activities in terms of the number of moles and volume of H$_2$ produced (n_{H_2}, v_{H_2}) are shown in Fig. S4.† For both PSs, H$_2$ production is effective and increasing the ratio PS/Cat notably increases the activity of the catalyst, as indicated by steadily higher TON$_{Cat}$ and TOF$_{Cat}$ values. Such behavior has been previously observed with the **Rubpy** (500 μM)/**Co**/H$_2$A/HA⁻ systems[50,51,53] and in many other H$_2$-evolving photocatalytic systems using Co[33,35,40,52,55–61] and Rh[20,34,62] based-molecular catalysts. Increasing the PS/Cat ratio indeed promotes the reduction of the catalyst. The increase in catalytic activity (in terms of TON$_{Cat}$ and TOF$_{Cat}$) induced by an increase in the PS/Cat ratio was well rationalized by a kinetic model recently reported by our group with the **Rubpy**/Co/HA⁻/H$_2$A photocatalytic system.[63] We showed that, in the case where PS degradation occurs, the limited TON$_{Cat}$ and TOF$_{cat}$ values are directly proportional to the PS/Cat ratio, even if other factors
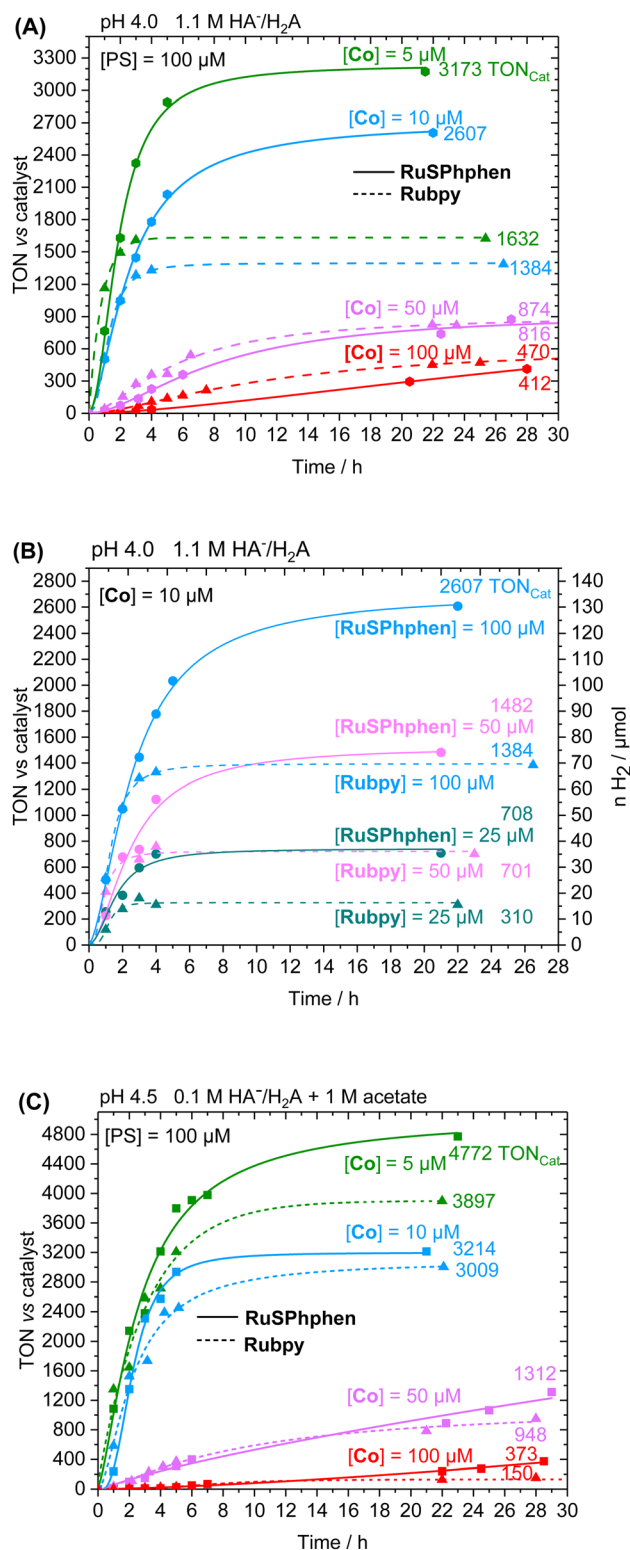

Fig. 2 Photocatalytic hydrogen production as a function of time in TON$_{Cat}$ under visible light irradiation (400–700 nm) from deaerated aqueous solutions (5 mL) of (A and B) NaHA (0.55 M) and H$_2$A (0.55 M) at pH 4.0 and (C) of NaHA (0.0714 M), H$_2$A (0.0286 M) and 1 M acetate buffer at pH 4.5, in the presence of a PS, **RuSPhphen** or **Rubpy** and the **Co** catalyst at various concentrations.

can also strongly impact the catalytic activity such as the kinetics of the PS degradation and all kinetics of electron transfer between SD, PS and Cat. In any case, lowering the catalyst concentration often has a deleterious impact on the stability of the photocatalytic system, as it also accelerates Ru PS decomposition (see below). At higher catalyst concentrations of 100 and 50 μM, thus a PS/Cat ratio of 1/1 and 2/1, the amount of H_2 produced is quite similar for both PSs after 28 h of irradiation with TON_{Cat} values of about 410 and 870, although the initial rate of H_2 production is higher for **Rubpy** (see TOF_{Cat} values in Table S3†). By contrast, a significant difference between the two PSs appears at lower catalyst concentrations of 10 and 5 μM, with the catalytic activity of **RuSPhphen** being much more effective with a production of H_2 multiplied by two (TON_{Cat} of about 2600 and 3170 for **RuSPhphen** at 10 and 5 μM, respectively *versus* 1380 and 1630 for **Rubpy**). However, the initial TOF_{Cat} values remain lower for **RuSPhphen** compared to

Rubpy. The higher H_2 production obtained with **RuSPhphen** can be directly correlated to the higher stability of the photocatalytic system under prolonged irradiation. Indeed, at catalyst concentrations of 10 and 5 μM, H_2 is produced for more than 10 h with **RuSPhphen** while H_2 evolution is fully stopped after only 3–4 h for **Rubpy**.

By monitoring the evolution of UV-vis absorption spectra under prolonged irradiation of solutions of **Rubpy** and **RuSPhphen** (100 μM), in the absence and in the presence of **Co** catalyst at 10 μM, it appears that **RuSPhphen** is more stable than **Rubpy**. Indeed, in the absence of catalyst, **Rubpy** is almost fully transformed after only 1 h (Fig. 3(A)). At this stage, the intensity of the initial visible band at 452 nm has decreased by more than 70% and is shifted to slightly higher wavelength, with the appearance of a new band at 462 nm associated with another one at about 350 nm (shoulder). These changes are characteristic of the formation of Ru-bis-bipyridine species by substitution of
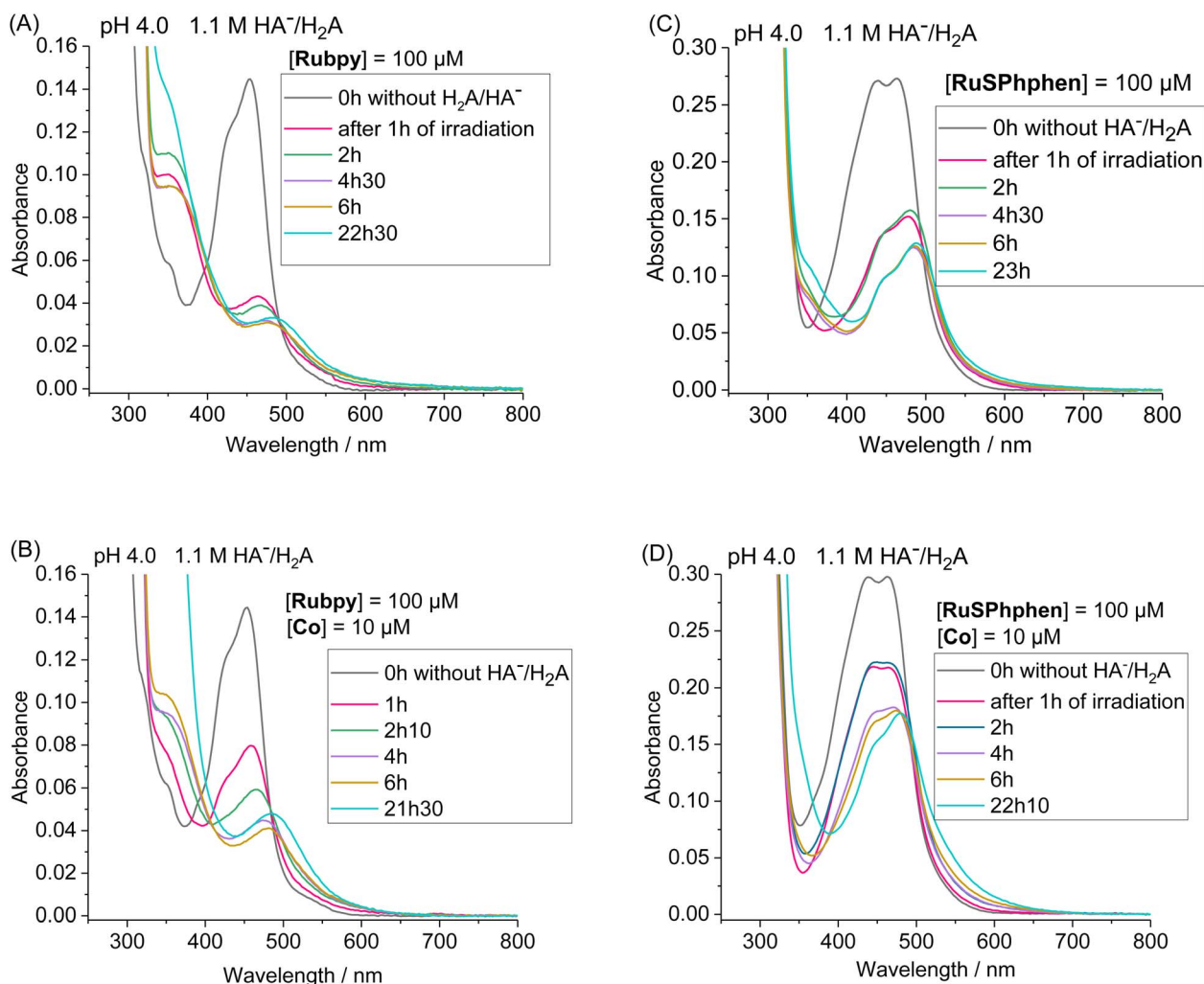

Fig. 3 Evolution of the UV/vis absorption spectra under continuous visible light irradiation ($\lambda = 400\text{--}700$ nm) of a deaerated 1.1 M HA^-/H_2A aqueous solution at pH 4.0 containing **Rubpy** (100 μM) in the absence (A) or in the presence of the **Co** catalyst (10 μM) (B) and **RuSPhphen** (100 μM) in the absence (C) and in the presence of the **Co** catalyst (10 μM) (D). UV/vis absorption spectra of initial solutions before irradiation containing a mixture of Ru PS/**Co** or Ru PS alone without HA^-/H_2A are shown in black lines and for (A) after 1 h, 2 h, 4 h 30 min, 6 h and 22 h 30 min of irradiation, for (B) 1 h, 2 h 10, 4 h, 6 h and 21 h 30 min, for (C) 1 h, 2 h, 4 h 30, 6 h and 23 h, and for (D) 1 h, 2 h, 4 h, 6 h and 22 h 10 min. Cell path length: $l = 1$ mm.

a bipyridine ligand by solvent molecules or anions, owing to the well-known poor stability of **Rubpy**$^{•-}$ in acidic water.[33,36,40,61] Early work by Sutin et al. showed that **Rubpy**$^{•-}$, generated by photolysis of an acidic aqueous solution of **Rubpy** and HA$^-$, undergoes a ligand substitution leading to the formation of $[Ru(bpy)_2(H_2O)_2]^+$ and the release of the protonated bipyridine ligand in solution.[36] Castellano et al. also demonstrated that an aqueous mixture of **Rubpy** and HA$^-$ at pH 4, under an irradiation at 452 nm, mainly results in the formation of $[Ru(bpy)_2(-HA)]^+$ along with side-products as $[Ru(bpy)_2(H_2O)_2]^{2+}$.[33]

This degradation can only be partially limited in the presence of 10 μM of catalyst, with the catalyst acting as a quencher of **Rubpy**$^{•-}$. Indeed, **Rubpy** is still present at about 50% of its initial amount after 1 h of irradiation but fully transformed after 4 h (Fig. 3(B)). This is consistent with the fact that the H$_2$ production has fully stopped after 3–4 h for 10 μM of catalyst (Fig. 2(A)).

Under similar conditions, **RuSPhphen** is much more stable in water in the presence of the catalyst (Fig. 3(D)). At least 75% of the initial PS is still present after 2 h of irradiation, and about 50–60% after 4–6 h (Fig. 3(D)) in agreement with H$_2$ production maintained with the same efficiency for at least 6 h (Fig. 2(A)). However, **RuSPhphen** doesn't seem much more stable than **Rubpy** in the absence of the catalyst, with degradation appearing almost complete after just 1 hour, since at this stage, the intensity of the band has decreased by half and the two maxima have shifted to the longer wavelengths (Fig. 3(C)).

We also performed control experiments. In the absence of the Ru PS or HA$^-$/H$_2$A, no H$_2$ is produced while the production of a small quantity of H$_2$ was detected for solutions containing only the Ru PS and HA$^-$/H$_2$A (Table S3†). The amount of H$_2$ produced, resulting from the direct reduction of protons by the reduced state of the Ru PS, is much lower than that in our previous experiments with a PS concentration of 500 μM.[40,50,51,53] It can be considered negligible at all catalyst concentrations as it represents a maximum of approximately 1% of the H$_2$ produced at a lower catalyst concentration of 5 μM (Table S3†). Also, addition of Hg in an experiment carried out with 100 μM **RuSPhphen** and 10 μM **Co** does not significantly change the photocatalytic activity (Fig. S5 and ESI†) ruling out the involvement of cobalt metallic colloids in H$_2$ production that would result from the decomposition of the cobalt complex.[64–66]

The good efficiency of the different systems at 100 μM prompts us to further decrease the concentration of PS to 50 and 25 μM. The concentration of the **Co** catalyst was fixed at 10 μM (Fig. 2(B)). Overall, decreasing the concentration of the PS, i.e. the PS/Cat ratio, notably decreases the activity of the catalyst and thus the H$_2$ production. Anyway, at this catalyst concentration, the H$_2$ production is always two times higher with **RuSPhphen** compared to **Rubpy** (TON$_{Cat}$ of 2600, 1480 and 708 for **RuSPhphen** at 100, 50 and 25 μM, respectively versus 1380, 700 and 310 for **Rubpy**), confirming once again the higher stability of photocatalytic systems with **RuSPhphen**. Indeed, it is interesting to see that even with these low concentrations of Ru, the production of H$_2$ is still effective after 6–12 h for **RuSPhphen** while that with **Rubpy** is stopped after 3–4 h.

Another set of experiments was performed with a concentration of sacrificial electron donor of 0.1 M of H$_2$A/HA$^-$ instead of 1.1 M. Under such conditions, the aqueous solution was buffered with 1 M acetate at pH 4.5 in order to keep the pH constant during the photocatalytic experiment. With a concentration of sacrificial electron donor divided by ten, a better stability of both Ru PSs is expected as the rate of formation of the reduced state, Ru$^{•-}$, subject to degradation by bidentate ligand dissociation, will be slower (see above). The photocatalytic performances of both Ru PSs at 100 μM in 1 M acetate buffer and 0.1 M HA$^-$/H$_2$A at pH 4.5 with 100, 50, 10 and 5 μM of **Co** catalyst are displayed in Fig. 2(C) and S4(B).† As anticipated, under such conditions, the photocatalytic systems are more stable, whatever the PS, with significantly higher TON$_{Cat}$ obtained at low **Co** concentrations compared to those obtained in 1.1 M HA$^-$/H$_2$A at pH 4.0. This is even more visible for **Rubpy** at low **Co** concentrations of 10 and 5 μM, with TONs$_{Cat}$ reaching up to 3010 and 3900, respectively after 22 h of irradiation versus 1380 and 1630 in 1.1 M H$_2$A/HA$^-$ (Fig. 2(A and C)). The stability of the photocatalytic system with **Rubpy** in 0.1 M H$_2$A/HA$^-$, 1 M acetate buffer is now approaching that of **RuSPhphen** with H$_2$ production still effective after 12 h leading to a less important difference in terms of TON$_{Cat}$ between the two PSs. Nevertheless, higher TON$_{Cat}$ values are obtained for **RuSPhphen** (4770, 3210, 1310, and 370 at 5, 10, 50, and 100 μM, respectively, versus 3900, 3010, 950, and 150 for **Rubpy**) with initial TOFs still higher for **Rubpy**. As observed in 1.1 M HA$^-$/H$_2$A at pH 4.0 (see above), the higher H$_2$ production in the case of **RuSPhphen** comes from the better stability of this PS versus **Rubpy**. From UV-visible absorption spectroscopy it is clear that the degradation of both PSs is slowed down either in the absence or in the presence of catalyst (10 μM) in 1 M acetate buffer with 0.1 M HA$^-$/H$_2$A (Fig. 4) compared to experiments performed in 1.1 M HA$^-$/H$_2$A (Fig. 3). Indeed, in the presence of catalyst, still about 50% of **Rubpy** and 75% of **RuSPhphen** are saved after about 6–8 h (Fig. 4(B and D)). The degradation of the PS is most probably the main limiting factor for H$_2$ production after long term irradiation. However, the accumulation of dehydroascorbic acid (DHA) in the course of the photocatalysis formed by the oxidation reaction of ascorbate is also known to progressively short-circuit the catalysis.[20,31,33,57,58,67,68] Dehydroascorbic acid is well-known to be a good electron acceptor able to prevent any electron transfer to the catalyst by trapping the electron from the reduced PS (see below).[31,57,58,67,68] Finally, it should be noticed that, in comparison with our previous photocatalytic systems using the **Co** catalyst, the TON$_{Cat}$ values measured here are very high, especially with the **RuSPhphen** (TON$_{Cat}$ of 3200 and 4770 at 10 and 5 μM of **Co** catalyst), and almost reach those obtained with the organic dye TATA$^+$ (TON$_{Cat}$ of 4080 and 5910 at 10 and 5 μM of **Co** catalyst), although the TATA$^+$ concentration was 500 μM.[40] It should also be noted that the TON$_{Cat}$ values obtained previously with the **Rubpy**/**Co**/HA$^-$/H$_2$A system (1.1 M or 0.1 M) for a **Rubpy** concentration of 500 μM never exceed 2000.[40,50,51,53] These results show that, in acetate buffer with 0.1 M HA$^-$/H$_2$A, it is possible to divide by five the quantity of the Ru PS, while
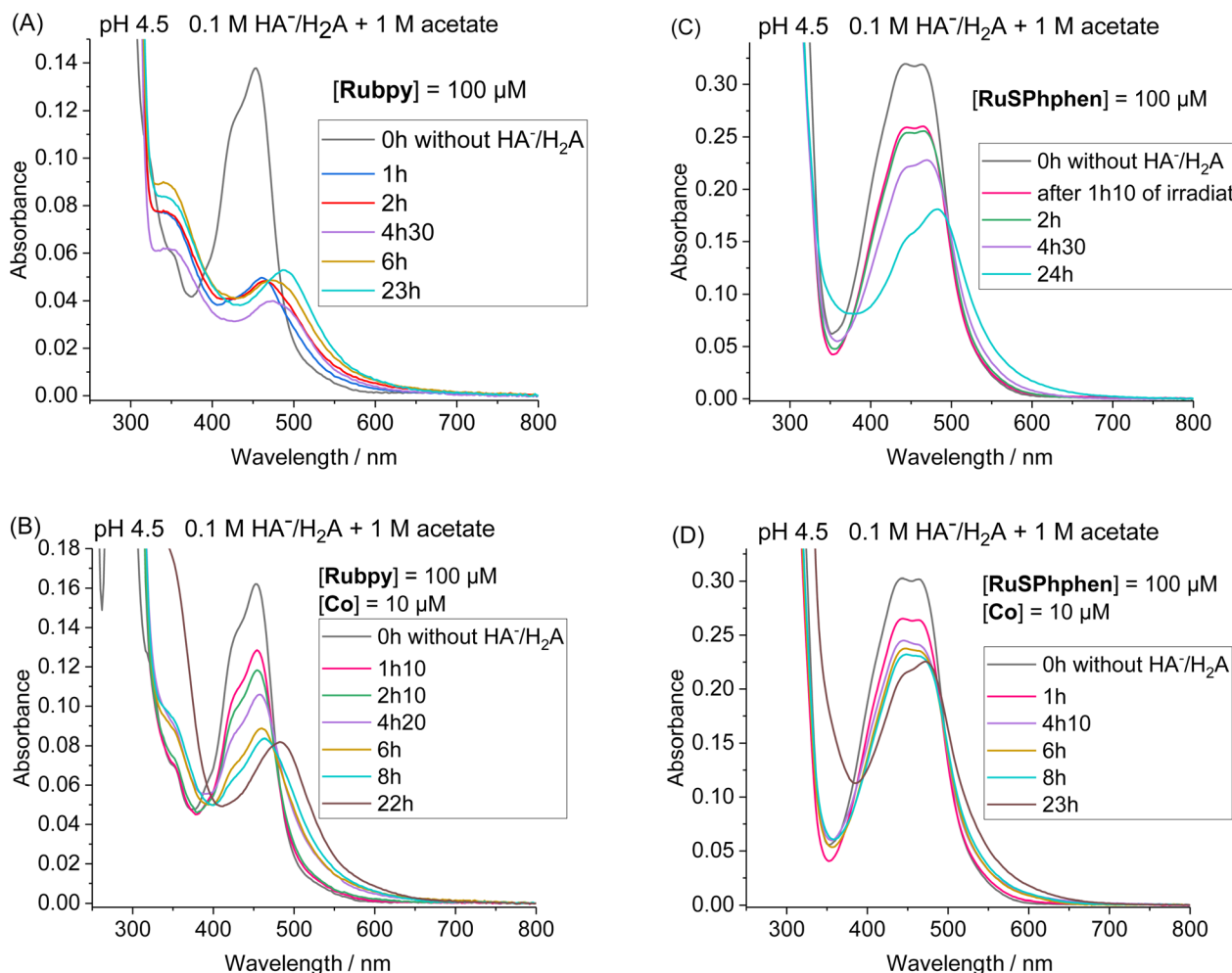
Fig. 4 Evolution of the UV/vis absorption spectra under continuous visible light irradiation ($\lambda = 400–700$ nm) of a deaerated 1 M acetate buffer containing 0.1 M HA$^-$/H$_2$A at pH 4.5 containing **Rubpy** (100 μM) in the absence (A) or in the presence of **Co** catalyst (10 μM) (B) and **RuSPhphen** (100 μM) in the absence (C) and in the presence of **Co** catalyst (10 μM) (D). UV/vis absorption spectra of initial solutions containing a mixture of Ru PS/**Co** or Ru PS alone without HA$^-$/H$_2$A are shown in black lines and for (A) after 1 h, 2 h, 4 h 30, 6 h and 23 h of irradiation, for (B) 1 h 10, 2 h 10, 4 h 20, 6 h, 8 h and 22 h, for (C) 1 h 10, 2 h, 4 h 30 and 24 h, and for (D) 1 h, 4 h 10, 6 h, 8 h and 23 h. Cell path length: $l = 1$ mm.
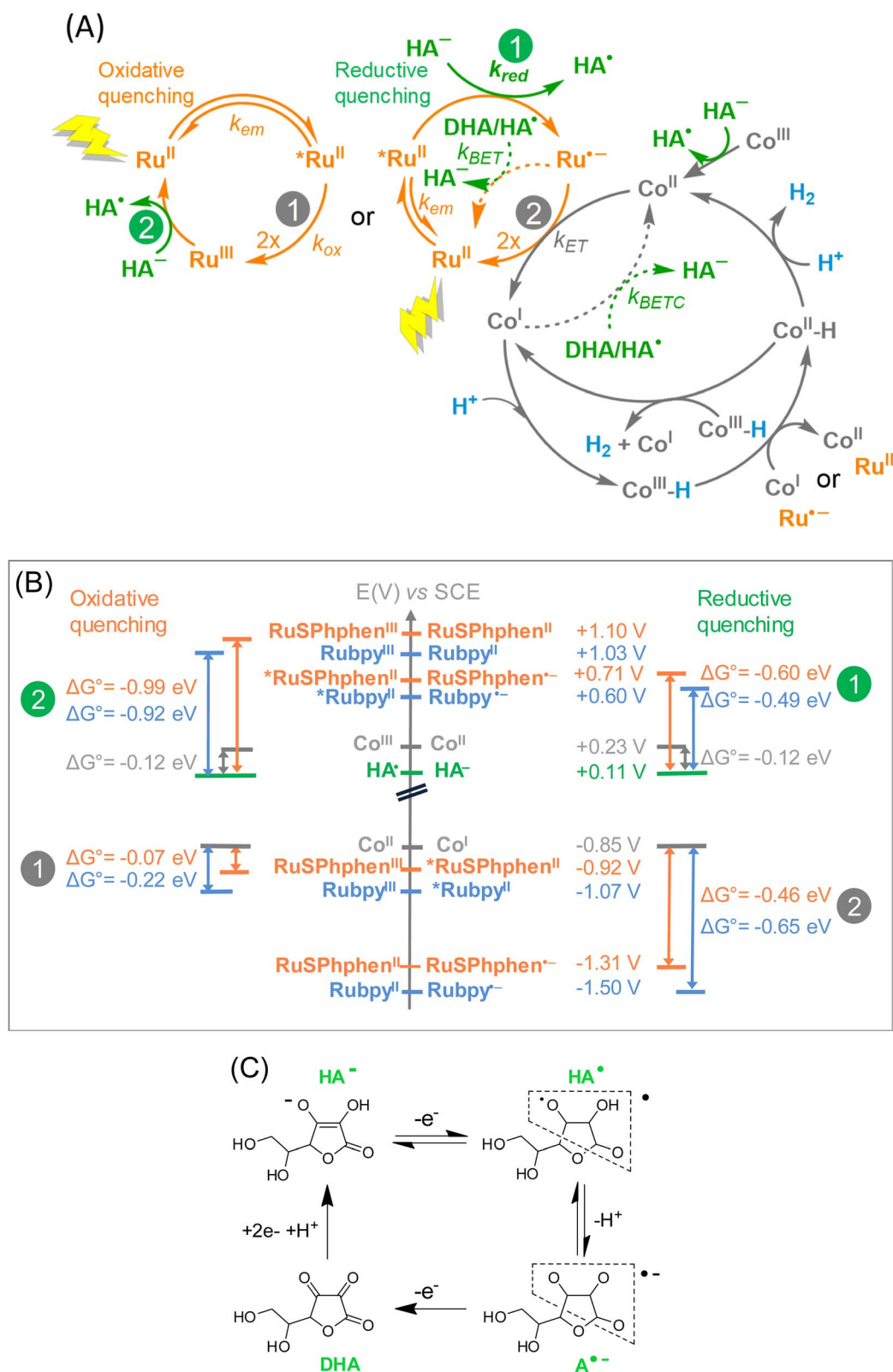
significantly improving the activity and thus saving precious metals.

Mechanistic insight for the RuSPhphen/Co/HA$^-$/H$_2$A system from photophysical measurements

The possible steps for the three-component photocatalytic system Ru/**Co**/HA$^-$/H$_2$A are depicted in Scheme 2(A). It should be mentioned that the **Co** catalyst, initially in the +III oxidation state is immediately reduced by ascorbate into its +II state (denoted **Co^{II}**), as previously shown.[50] Thus, the cobalt species that enters the photocatalytic cycle is **Co^{II}**. The photocatalytic cycle is initiated by the absorption of one photon by the Ru PS under visible light irradiation generating the excited state of the PS, denoted as *Ru^{II}. Due to the large excess of HA$^-$ *versus* the catalyst, *Ru^{II} is generally quenched by an electron transfer from HA$^-$ (reductive quenching), generating Ru$^{•-}$ and the oxidized form of ascorbate, HA$^{•}$. Ru$^{•-}$ is a good reductant (Table S1†) that can in turn reduce the **Co^{II}** catalyst into **Co^{I}**,

reforming the initial state of the PS, Ru^{II}. HA$^{•}$ can easily release a proton to form A$^{•-}$, an unstable species which easily disproportionates to generate DHA (Scheme 2(C)). DHA is a very good electron acceptor able to withdraw electrons from Ru$^{•-}$ and/or the reduced catalyst **Co^{I}** (Scheme 2(A)). Therefore, when DHA accumulates in solution in the course of the catalysis, the latter is short-circuited by back electron transfers that occur from Ru$^{•-}$ to HA$^{•}$ or DHA (BET process), restoring Ru^{II} and HA$^-$, and from **Co^{I}** to HA$^{•}$ or DHA (BETC process), reforming **Co^{II}**. In other words, if the BET and BETC processes dominate over the catalytic process due to the accumulation of DHA, H$_2$ generation is stopped. The other possibility is the quenching of *Ru^{II} by an electron transfer to the **Co^{II}** catalyst (oxidative quenching), generating Ru^{III} and the one-electron reduced catalyst, **Co^{I}**, but this process is usually less favourable (see below). Then the **Co^{I}** species can react with protons to form the elusive Co^{III} hydride species (denoted as **Co^{III}-H**) from which H$_2$ can be released following different mechanisms that

Scheme 2   (A) Possible mechanisms for the light-driven H₂ production with the system Ru/**Co**/HA⁻/H₂A (Ru = **Rubpy** or **RuSPhphen**). (B) Diagrams of potentials referred *versus* SCE for the redox couples of **RuSPhphen** and **Rubpy** PSs at the ground and excited states, the [Co(CR14)Cl₂]⁺ (**Co**) catalyst, and HA⁻. (C) Oxidation processes of ascorbate salt (HA⁻) to dehydroascorbic acid (DHA) and back reduction of DHA to HA⁻.

could proceed in parallel and that are difficult to demonstrate experimentally.[50] Reduction of **Co^{III}-H** into **Co^{II}-H** by another **Co^I** or by **Ru$^{\cdot-}$** is the most probable mechanism.[50] **Co^{II}-H** can then produce H$_2$ by reacting with a proton or another **Co^{II}-H** present in solution.[69]

Experimentally, we observed that, whatever the concentration of HA$^-$/H$_2$A, the systems with **RuSPphen** are significantly more efficient than the corresponding systems with **Rubpy**. The enhanced activity can be attributed to the higher stability of **RuSphen** in acidic water compared to the regular **Rubpy** that could be the result of several parameters:

(i) a higher intrinsic stability of the reduced state, **RuSPphen$^{\cdot-}$**, in acidic water, compared to **Rubpy$^{\cdot-}$**, due to the steric hindrance of the SPhphen ligand,[70] and/or a greater delocalization of the radical anion over the reduced **SPhphen** ligand making it less prone to decoordination,

(ii) a faster electron transfer from **RuSPphen$^{\cdot-}$** to the catalyst (ET process), and/or

(iii) a faster back electron transfer from **RuSPphen$^{\cdot-}$** to HA$^{\cdot}$ or DHA (BET process).

UV-visible absorption spectra recorded in the course of the photocatalysis (Fig. 3 and 4) do not give any information at this stage because only the ground state of the PSs is observed. The two last possibilities (ii) and (iii) do not necessarily require a better intrinsic stability of **RuSPphen$^{\cdot-}$** compared to that of **Rubpy$^{\cdot-}$**. Further information can be obtained by the determination of the rate constants of the intermolecular electron transfers by time-resolved luminescence and nanosecond transient absorption spectroscopy thanks to the detection of the key intermediates ***RuSPphen** and **RuSPphen$^{\cdot-}$** and the reduced form of the catalyst, **Co^I**.
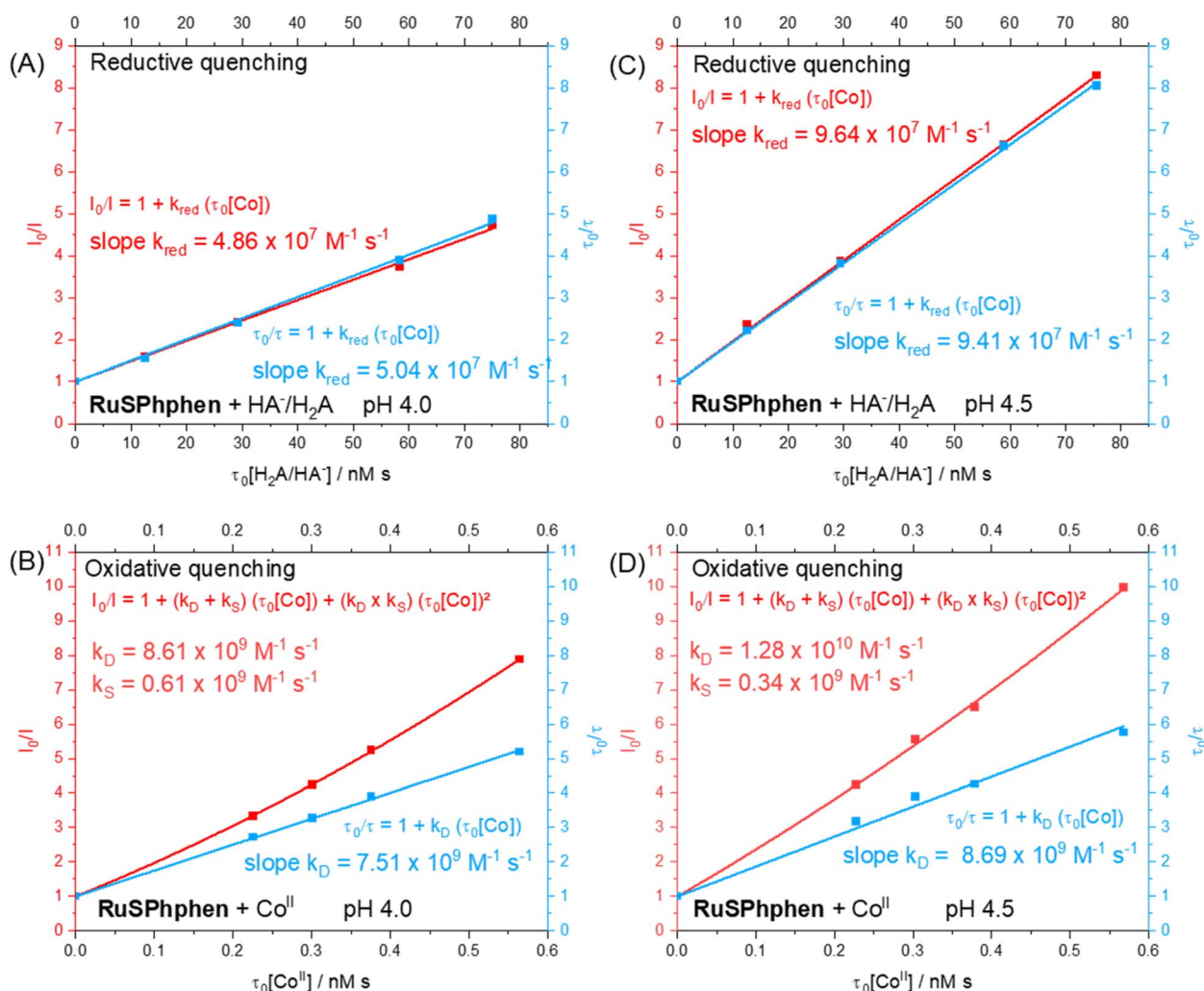

Fig. 5 Stern–Volmer plot obtained by stationary (I_0/I, red trace) and time-resolved (τ_0/τ, blue trace) luminescence spectroscopies in deaerated aqueous solution at pH 4.0 (A and B) and 4.5 (C and D) (0.1 M acetate buffer) for the reductive quenching of **RuSPphen** (3.4 μM) at the excited state by the NaHA/H$_2$A couple by varying their total concentration (0, 3.3, 7.7, 15.4 and 19.8 mM) (A and C) and for the oxidative quenching of **RuSPphen** (3.4 μM) at the excited state by **Co^{II}** (*i.e.* [Co^{II}(CR14)(H$_2$O)$_2$]$^{2+}$) by varying its concentration (0, 0.06, 0.08, 0.1 and 0.15 mM) (B and D). I and I_0 are respectively the emission intensities of ***RuSPphen** registered at 614 nm with an excitation at 462 nm, with or without NaHA/H$_2$A or **Co^{II}**. τ and τ_0 are respectively the lifetimes of ***RuSPphen** registered at 614 nm with an excitation at 409 nm, with or without NaHA/H$_2$A or **Co^{II}**. The lifetime of ***RuSPphen** without NaHA/H$_2$A or **Co^{II}** (τ_0) was determined to be 3.79 μs (A), 3.76 μs (B), 3.82 μs (C) and 3.79 μs (D).

We can first estimate the driving force for the oxidative and reductive quenching processes of *Ru from the standard potentials at the ground and excited states of HA[−], **Rubpy**, **RuSPhphen** and **Co** (Table S1,† and Scheme 2(B)). The standard potentials of **RuSPhphen** at the ground and excited states have only been obtained in DMF. We hypothesized that these values are close to those in water and used these values to calculate the driving force in water converted *versus* the SCE reference electrode by adding 298 mV (Table S1†). The reduction of the **Co**[II] catalyst by **RuSPhphen**[•−] (reductive quenching mechanism) and by *RuSPhphen (oxidative quenching mechanism) are both thermodynamically favorable reactions (Scheme 2(B)). Indeed, considering the reduction potential of **Co** ($E_{1/2}$ (Co[II]/Co[I]) = −0.85 V *vs.* SCE) in water and the redox potential of **RuSPhphen** at reduced and excited states ($E_{1/2}$ (Ru[II]/Ru[•−]) = −1.31 V and $E_{1/2}$ (Ru[III]/*Ru) = −0.92 V *vs.* SCE, Scheme 2), the driving force (ΔG_0) is exergonic with values of −0.46 and −0.07 eV, respectively for the **Co**[II] reduction by Ru[•−] and *Ru. The activation of the **Co** H₂-evolving catalyst by **RuSPhphen** is thus thermodynamically possible.

In order to identify the most favourable first step of the photocatalytic mechanism (reductive *vs.* oxidative quenching of *RuSPhphen), Stern–Volmer plots were plotted between **RuSPhphen** and HA[−]/H₂A (Fig. 5(A and C)) and between **RuSPhphen** and **Co** (Fig. 5(B and D)), in aqueous solution at pH 4.0 (Fig. 5(A and B)) and 4.5 (Fig. 5(C and D)), respectively. Stern–Volmer plots were obtained *via* stationary (I_0/I) and time-resolved (τ_0/τ) luminescence spectroscopies in order to survey the dynamic quenching of *Ru by HA[−] and **Co** and also to characterize a possible static quenching that could occur between *Ru, HA[−] and **Co**, during photocatalysis.[71] The rate

constants for the reductive quenching (k_{red}) of *RuSPhphen by HA[−] were determined from τ_0/τ values to be 5.04×10^7 at pH 4.0 and 9.41×10^7 at pH 4.5. These rate constants are higher than those reported with the reference PS **Rubpy** under similar conditions (Table 1; 2×10^7 M^{−1} s^{−1} at pH 4.0 (ref. 72 and 73) and 1×10^7 M^{−1} s^{−1} at pH 4.5 (ref. 72)). Of note, k_{red} constants between *Ru and HA[−] determined from I_0/I values (4.86×10^7 at pH 4.0 and 9.64×10^7 at pH 4.5) are very close to those estimated from τ_0/τ values (Fig. 5(A and C)), which indicates that only dynamic quenching occurs between these two species, thus ruling out a static quenching and an interaction even weaker between *RuSPhphen and HA[−]. It is interesting to note that a higher rate constant was observed by the Brewer's group for reductive quenching (2.9×10^9 M^{−1} s^{−1} by HA[−] in water) of a Ru PS within the triad [{(SO₃Ph)₂phenRu(dpp)}RhX₂]⁵⁺, having two 4,7-diphenyl-1,10-phenanthroline 4′,4″-disulfonate ligands on the Ru units (Scheme 1).[49] Castellano's group also reported a high rate constant (4.9×10^9 M^{−1} s^{−1}) for reductive quenching between **RuPhphen** and DMT as a SD (see above), which was attributed to the long lifetime of the PS's excited state (5.86 μs) that facilitates bimolecular electron-transfer reactions.[42]

For the oxidative quenching of *RuSPhphen by **Co**[II] (Table 1), rate constants (k_{ox}) of 7.51×10^9 M^{−1} s^{−1} at pH 4.0 and 8.69×10^9 M^{−1} s^{−1} at pH 4.5 were estimated from τ_0/τ values, the latter being higher than those reported by our group with **Rubpy** at pH 4.0 (5.1×10^9 M^{−1} s^{−1}) and measured herein at pH 4.5 (1.27×10^9 M^{−1} s^{−1}, Fig. S7†). In addition, upward-curving Stern–Volmer plots were obtained from I_0/I values for the oxidative quenching of *RuSPhphen by **Co**[II] at pHs 4.0 and 4.5 (Fig. 5(B and D)), which deviates from the linear plots obtained from τ_0/τ values. This behaviour clearly indicates that both static and

Table 1 Time and rate constants measured by time-resolved emission and transient absorption spectroscopies in deaerated aqueous solutions containing **RuSPhphen** or **Rubpy** in the presence of the NaHA/H₂A couple and/or the **Co** catalyst under the experimental conditions described below; optical path = 1 cm

	RuSPhphen (3.4 μM)	**Rubpy** (10 μM)	**RuSPhphen** (3.4 μM)	**Rubpy** (83 or 10 μM)
PS	0.1 M acetate buffer at pH 4.0		0.1 M acetate buffer at pH 4.5	
τ(*Ru) without HA[−]/Co[II][c]	4 μs	0.6 μs	3.8 μs	0.6 μs
k_{red} with HA[−]	5.04×10^7 M^{−1} s^{−1}	2×10^7 M^{−1} s^{−1} (ref. 72 and 73)	9.41×10^7 M^{−1} s^{−1}	1×10^{7a} M[−1] s^{−1} (ref. 72)
k_{ox} with Co[II][c]	9.22×10^{9d} M[−1] s^{−1}	5.1×10^{9e} M[−1] s^{−1} (ref. 50)	1.34×10^{10d} M[−1] s^{−1}	$7.07 \times 10^{9b,d}$ M[−1] s^{−1}
	RuSPhphen (50 μM)	**Rubpy** (130 μM)	**RuSPhphen** (50 μM)	**Rubpy** (100 μM)
PS	1.1 M HA[−]/H₂A pH 4.0		0.1 M HA[−]/H₂A, 1 M acetate pH 4.5	
k_{BET} with HA[−]	2.10×10^{10} M^{−1} s^{−1}	3.5×10^9 M^{−1} s^{−1} (ref. 51)	1.47×10^{10} M^{−1} s^{−1}	7.4×10^9 M^{−1} s^{−1} (ref. 77)
k_{ET} with HA[−]/Co	2×10^9 M^{−1} s^{−1} [Co] = 200 μM	1.4×10^9 M^{−1} s^{−1} (ref. 51) [Co] = 240 μM	3.3×10^9 M^{−1} s^{−1} [Co] = 200 μM	n.d.
k_{diss}[f] with HA[−]/Co	4.68×10^3 s^{−1} [Co] = 200 μM	2.6×10^3 s^{−1} (ref. 51) [Co] = 240 μM	7.11×10^3 s^{−1} [Co] = 200 μM	n.d.

[a] Measured with [**Rubpy**] = 83 μM. [b] Measured with [**Rubpy**] = 10 μM. [c] The Co[II] species (*i.e.* [Co[II](CR14)(H₂O)₂]²⁺) used for the Stern–Volmer plot was obtained by exhaustive electrolysis at −0.20 V *vs.* Ag/AgCl of an aqueous solution (0.1 M NaClO₄, pH 4.5) of 0.5 mM [Co[III](CR14)Cl₂]⁺. [d] Global rate constant of oxidative quenching (k_{ox}) as the sum of static and dynamic quenching ($k_S + k_D$). [e] k_{ox} was only estimated by the authors from τ_0/τ, *i.e.* from the rate constant of dynamic quenching (k_D). [f] k_{diss} is the kinetic constant related to the disappearance of Co[I] in solution and can be expressed as $k_1[H^+] + k_{betc}[HA^•]$. n.d.: not determined.

dynamic quenching are involved in the disappearance of *RuSPhphen.[71,74–76] The static quenching can be ascribed to a potential coulombic interaction between the negatively charged *RuSPhphen (beared on the sulfonate groups) and the positively charged Co[II] catalyst that favors the formation of an ion pair and then significantly increases the kinetics of electron transfer from *RuSPhphen to Co[II]. Classically, the upward curvature of the Stern–Volmer plot (*i.e.* $I_0/I = f(\tau_0[Q])$, where [Q] is the quencher concentration) is fitted with a polynomial function of the second order, from which the static and dynamic quenching rate constants (k_S and k_D) are extracted by solving a quadratic equation (see Fig. 5 and the section devoted to the Stern–Volmer plot in the ESI†).[71] So, from the polynomial fitting, k_S and k_D values for the oxidative quenching of *RuSPhphen by Co[II] were determined to be respectively 0.61×10^9 and 8.61×10^9 M^{-1} s^{-1} at pH 4.0, and respectively 0.34×10^9 and 1.28×10^{10} M^{-1} s^{-1} at pH 4.5. If we consider that the global rate constant of the oxidative quenching (k_{ox}) is the sum of k_S and k_D, the k_{ox} values are estimated to be 9.22×10^9 M^{-1} s^{-1} at pH 4.0 and 1.32×10^{10} M^{-1} s^{-1} at pH 4.5 (Table 1). The small contribution of static quenching (k_S) at both pHs (6.6% at pH 4.0 and 2.6% at pH 4.5) to the global rate constant k_{ox} suggests that the phenomenon of ion pairing between *RuSPhphen and Co[II] is weak. Importantly, a deviation is also observed from the linear Stern–Volmer plot obtained between *Rubpy and Co[II] at pH 4.5, also suggesting a mixture of static and dynamic quenching, even if the global rate constant (k_{ox} = 7.07×10^9 M^{-1} s^{-1}) remains lower than those between *RuSPhphen and Co[II] (Fig. S7†).

Considering the concentrations of Co catalyst (5–100 μM) and HA$^-$/H$_2$A (0.1 and 1.1 M) used during photocatalysis and the second order rate constants estimated above from τ_0/τ, the reductive quenching of *RuSPhphen dominates over the oxidative one at both pHs with respective pseudo-first order rate constants of 5.54×10^7 s^{-1} *vs.* 4.6–92.2×10^4 s^{-1} at pH 4.0, and of 9.47×10^6 s^{-1} *vs.* 6.7–134×10^4 s^{-1} at pH 4.5. Regarding our study, the difference in the kinetic constants observed between the two PSs cannot be explained by the driving forces of the two quenching processes (Scheme 2(B)). Indeed, the driving force $\Delta G°$ for the oxidative quenching is lower for RuSPhphen (-0.07 eV) compared to Rubpy (-0.22 eV), while the driving force for the reductive quenching for both PSs is of the same order of magnitude (-0.60 eV for RuSPhphen and -0.49 eV for Rubpy). Thus, the higher rate constants of both reductive and oxidative quenching processes for *RuSPhphen could then be ascribed to its much longer lifetime (3.8 μs) compared to that of *Rubpy (0.6 μs) (Table S2†),[62] promoting bimolecular electron transfer both with HA$^-$ and Co[II].

The photocatalytic mechanism of the system RuSPhphen/Co/HA$^-$/H$_2$A was further investigated *via* transient absorption spectroscopy. In the absence of the Co catalyst, the transient absorption spectra of aqueous solutions of RuSPhphen (50 μM) and HA$^-$/H$_2$A (1.1 M for pH 4.0 and 0.1 M for pH 4.5), after a flash excitation at 462 nm, exhibit the characteristic absorption band of RuSPhphen$^{•-}$ at 510–520 nm (MLCT transition) and *ca.* 350 nm (π–π* transition) (Fig. 6). An additional transition related to RuSPhphen$^{•-}$ is observed at *ca.* 700 nm which

could be ascribed to a d–d transition. This transition at 700 nm is also observed in the absorption spectrum of RuSPhphen$^{•-}$ generated by an exhaustive reduction in DMF (Fig. 1(B)).

The generation of RuSPhphen$^{•-}$ through a photo-induced electron transfer from HA$^-$ to *RuSPhphen is complete within 0.4 μs following the laser excitation (Fig. 6). The decay of RuSPhphen$^{•-}$, monitored *via* the transient trace at 510 nm (Fig. S8†), can be fitted with a second-order kinetic law (eqn (3)) and its concentration tends to zero after almost 300 μs. A second-order kinetics can be employed to analyse the RuSPhphen$^{•-}$ decay since the latter stems from the back-electron transfer between RuSPhphen$^{•-}$ and one of the oxidized forms of ascorbate (*i.e.* HA$^•$ or DHA), and the concentrations of RuSPhphen$^{•-}$ and HA$^•$ (or DHA) are assumed to be equal:

$$\frac{1}{[\text{Ru}^{•-}]} = \frac{1}{[\text{Ru}^{•-}]_0} + k_{BET}t \tag{3}$$

where k_{BET} is the bimolecular rate constant of the back-electron transfer. The concentration [Ru$^{•-}$] could be converted to the variation of absorption at 510 nm in the transient absorption spectra *via* the Beer–Lambert law, giving the new eqn (4):

$$\frac{1}{\Delta A} = \frac{1}{\Delta A_0} + k_{obs}t \tag{4}$$

where ΔA_0 is the maximum of RuSPhphen$^{•-}$ absorption at 510 nm after the laser excitation. The observable constant k_{obs}, which is equal to $k_{BET}/\Delta \varepsilon$, was determined as the slope of the linear function $1/\Delta A$ plotted as a function of time to 1.15×10^6 s^{-1} with 0.1 M HA$^-$/H$_2$A (pH 4.5) and 1.6×10^6 s^{-1} with 1.1 M HA$^-$/H$_2$A (pH 4.0) (Fig. S8(A and C)†). Similar or close values of k_{obs} have been calculated by monitoring the absorption changes at 700 nm (Fig. S8(B and D)†). Assuming a $\Delta \varepsilon$ value of 1.28×10^4 M^{-1} cm^{-1} at 510 nm for the RuSPhphen$^{•-}$ species,[78] the k_{BET} constant is estimated to be 1.47×10^{10} M^{-1} s^{-1} with 0.1 M HA$^-$/H$_2$A and 2.1×10^{10} M^{-1} s^{-1} with 1.1 M HA$^-$/H$_2$A. Such rate constants are very high and close to the diffusion limit in solution. These values are higher than those measured between Rubpy$^{•-}$ and HA$^•$ under similar experimental conditions (7.4×10^9 M^{-1} s^{-1} with 0.1 M HA$^-$/H$_2$A[77] and 3.5×10^9 M^{-1} s^{-1} with 1.1 M HA$^-$/H$_2$A;[51] Table 1). Given the instability of the reduced state Ru$^{•-}$ in water, this faster back electron transfer, regenerating the initial RuSPhphen, could explain the greater stability of this PS compared to Rubpy during photocatalysis. Of note, a high value of k_{BET} (7.7×10^9 M^{-1} s^{-1}) between RuPhphen$^{•-}$ and DMT$^{•+}$ has also been observed by Castellano *et al.*, indicating that this family of Ru PS with bathophenanthroline ligands is subject to fast bimolecular electron transfers.[42]

In the presence of a catalyst, the transient absorption spectra of the aqueous solutions containing RuSPhphen (50 μM), Co (200 μM) and HA$^-$/H$_2$A (1.1 M for pH 4.0 and 0.1 M for pH 4.5) also present the characteristic signature of RuSPhphen$^{•-}$ at 350, 510 and 700 nm (Fig. 7), confirming a reductive quenching of *RuSPhphen by HA$^-$. As observed above with the simple mixture of RuSPhphen and HA$^-$/H$_2$A, the growth of the RuSPhphen$^{•-}$ absorption bands at 510 nm in the presence of Cat and SD still occurs within the first 0.4 μs after the laser flash. The decay of RuSPhphen$^{•-}$ in the presence of Co and HA$^-$,
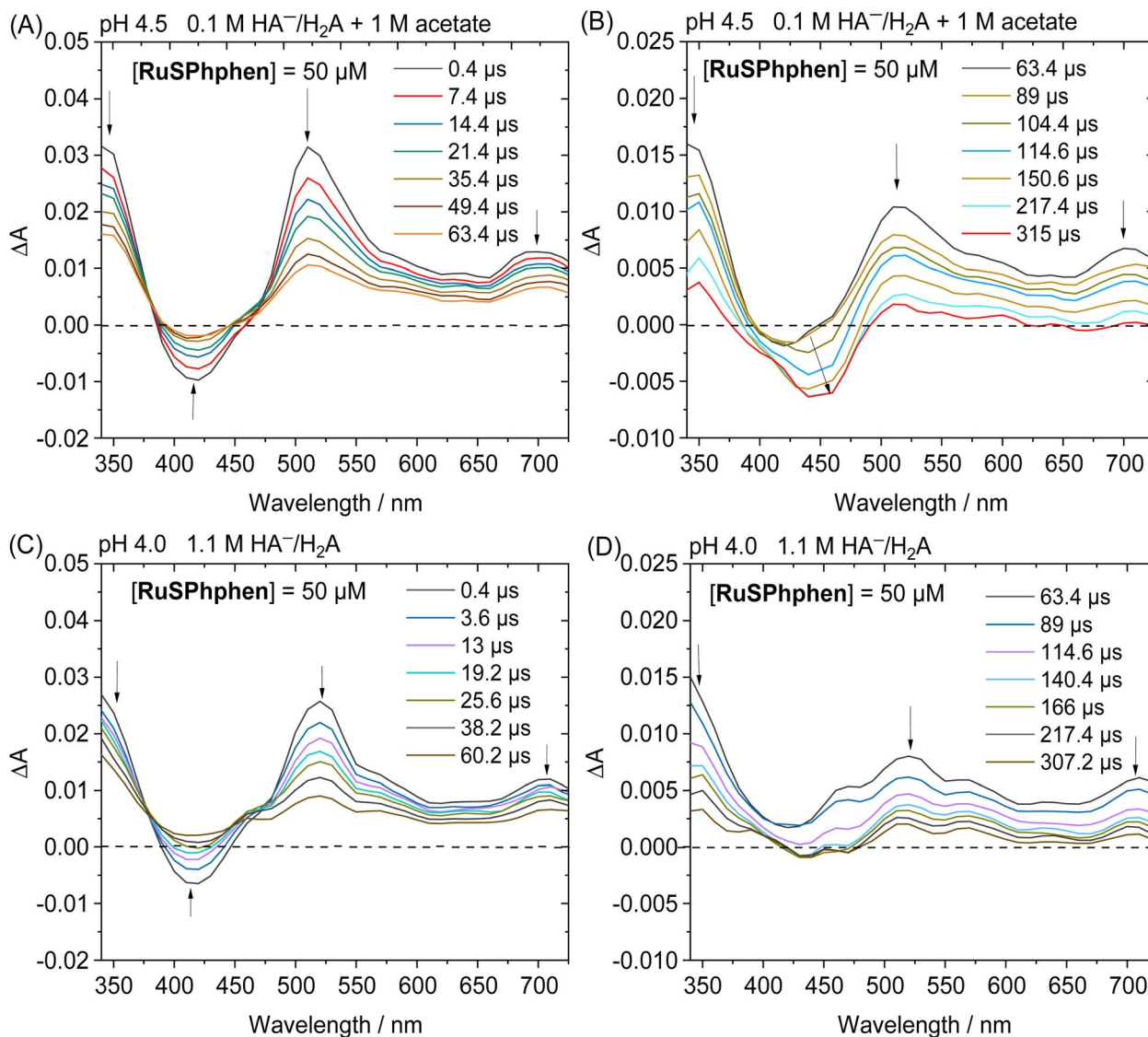
Fig. 6 Transient absorption spectra after laser excitation ($\lambda = 462$ nm) of (A and B) a deaerated aqueous solution of 1 M acetate buffer and NaHA/H$_2$A (0.1 M) at pH 4.5 containing **RuSPhphen** (50 μM) within the time ranges 0.4–63.4 μs (A) and 63.4–315 μs (B), and (C and D) a deaerated aqueous solution at pH 4.0 containing NaHA/H$_2$A (1.1 M) and **RuSPhphen** (50 μM) within the time ranges 0.4–60.2 μs (C) and 63.4–307.2 μs (D); optical pathlength = 1 cm.

observed in the transient absorption spectra (Fig. 7) and the transient absorption trace at 510 nm (Fig. S9(A and B)†), is complete after *ca.* 8 μs, which is much faster than that observed without catalyst (after *ca.* 300 μs, Fig. 6 and S8†). Considering that the decay of **RuSPhphen**$^{\bullet-}$ is mainly due to an electron transfer towards the **Co** catalyst present in large excess in solution (200 μM), the latter can be fitted with a pseudo first order kinetic law following eqn (5):

$$\ln[\text{Ru}^{\bullet-}] = \ln[\text{R}^{\bullet-}]_0 - k_{\text{obs}}t \tag{5}$$

Considering the Beer–Lambert law, the **RuSPhphen**$^{\bullet-}$ concentration (*i.e.* [Ru$^{\bullet-}$]) could be converted to the variation of

absorption at 510 nm in the transient absorption spectra following eqn (6):

$$\ln \Delta A = \ln \Delta A_0 - k_{\text{obs}}t \tag{6}$$

where the observable rate constant k_{obs} is equal to $k_{\text{ET}} \times$ [Co]; k_{ET} being the rate constant of electron transfer from **RuSPhphen**$^{\bullet-}$ to **Co$^{\text{II}}$** and [Co] being the concentration of the cobalt catalyst (200 μM), considered as a constant due to its large excess compared to Ru$^{\bullet-}$ generated during photocatalysis. k_{obs} can thus be determined as the slope of the linear function $\ln(\Delta A)$ plotted as a function of time. Values of 6.6×10^5 s^{-1} with 0.1 M HA$^-$/H$_2$A (pH 4.5) and 4.04×10^5 s^{-1} with 1.1 M HA$^-$/H$_2$A (pH 4.0) have been then determined (Fig. S9(A and B)†). Considering a **Co** concentration of 200 μM, the rate constant k_{ET}
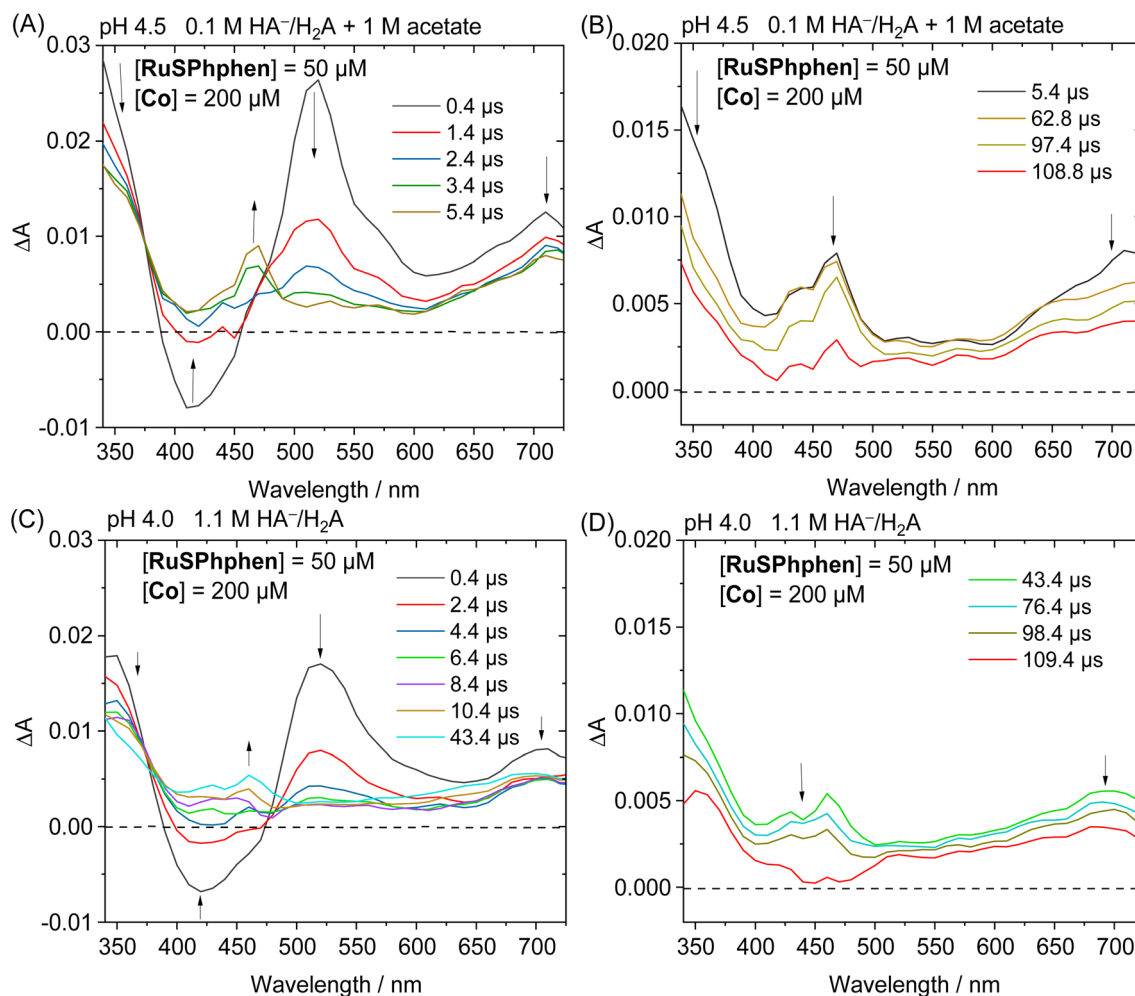
Fig. 7 Transient absorption spectra after laser excitation ($\lambda = 462$ nm) of (A and B) a deaerated aqueous solution of 1 M acetate buffer and NaHA/H$_2$A (0.1 M) at pH 4.5 containing **RuSPhphen** (50 μM) and **Co** (200 μM) within the time ranges 0.4–5.4 μs (A) and 5.4–108.8 μs (B) and (C and D) a deaerated 1.1 M NaHA/H$_2$A aqueous solution at pH 4.0 containing **RuSPhphen** (50 μM) and **Co** (200 μM) within the time ranges 0.4–43.4 μs (C) and 43.4–109.4 μs (D); optical pathlength = 1 cm.

is estimated to be 3.3×10^9 M^{-1} s^{-1} with 0.1 M HA$^-$/H$_2$A at pH 4.5 and 2.0×10^9 M^{-1} s^{-1} with 1.1 M HA$^-$/H$_2$A at pH 4.0 (Table 1). Both rate constants are quite high, attesting to a fast electron transfer from **RuSPhphen$^{\bullet-}$** to the cobalt catalyst. Electron transfer kinetics with a similar order of magnitude have been reported by Castellano's group from **RuPhphen$^{\bullet-}$** to the cobalt(III) glyoxime catalyst (2.4×10^9 M^{-1} s^{-1})[42] and by other groups from **Rubpy$^{\bullet-}$** to cobalt catalysts with various polypyridine ligands (1.4–5.7×10^9 M^{-1} s^{-1}).[33,58,59,72,79] Besides, a slightly lower k_{ET} constant of 1.4×10^9 M^{-1} s^{-1} has been previously reported by our group with the photocatalytic system **Rubpy**/Co/HA$^-$/H$_2$A (1.1 M) at pH 4.0,[51] which suggests that the reducing powers of **RuSPhphen** and **Rubpy** at the reduced state are close in aqueous solution. So, the greater stability of the photocatalytic system using **RuSPhphen** cannot be explained by a faster electron transfer from Ru$^{\bullet-}$ to Co^{II} compared to **Rubpy**. These close k_{ET} values between the reduced states of PSs, **RuSPhphen$^{\bullet-}$** and **Rubpy$^{\bullet-}$**, and Co^{II} also confirm that only a weak interaction *via* ion pairing is present between these

species, even with **RuSPhphen** which exhibits six negatively charged sulfonate groups (see the above discussion on oxidative quenching).

In parallel with the disappearance of **RuSPhphen$^{\bullet-}$** observed at 510 and 700 nm in the transient absorption spectra, the appearance of **Co^I**, which is the result of an electron transfer from **RuSPhphen$^{\bullet-}$** to **Co^{II}**, is observed through the growth of two bands at about 430 and 460 nm and a large band at above 550 nm along with a maximum at 700 nm (Fig. 7). The same spectroscopic signature for the reduced form of the catalyst, **Co^I**, was previously observed by transient absorption spectroscopy in the presence of the organic dye TATA$^+$ and 0.1 M HA$^-$/H$_2$A at pH 4.5.[40] The formation and the disappearance of the **Co^I** species can be observed by monitoring the transient trace at 700 nm, but the changes in this band are quite complex (Fig. S10(A and D)†). First, a very fast decrease is observed at 700 nm with time constants of 89.9 ns with 0.1 M HA$^-$/H$_2$A and 14.1 ns with 1.1 M HA$^-$/H$_2$A (Fig. S10(B and E),† respectively), the latter being mainly ascribed to the disappearance of Ru$^{\bullet-}$

which exhibits an absorption band at this wavelength. Following this fast decay, new growth of the band at 700 nm occurs within a time scale of 20 μs (Fig. S10(A and D)†), along with a change of the shape of the absorption band between 550 and 725 nm observed in the transient absorption spectra (Fig. 7(A and C)). This band growth is related to the formation of Co^I. Then, this band at 700 nm undergoes a decrease due to an oxidative protonation of Co^I generating the Co^{III}-H hydride species, the key intermediate for H_2 evolution (Scheme 2(A)).

This decay at 700 nm, 20 μs after the flash excitation, can be analysed via a pseudo-first order kinetic law (eqn (6)), since the concentration of the proton source (i.e. $0.55 > [H_2A] > 0.03$ M) is in large excess compared to that of the Co^I species. The k_{obs} rate constant for the formation of the Co^{III}-H hydride species can be determined as the slope of the linear function $\ln(\Delta A)$ plotted as a function of time (vide supra), which gives values of 7.11×10^3 s^{-1} with 0.1 M HA^-/H_2A (pH 4.5) and 4.68×10^3 s^{-1} with 1.1 M HA^-/H_2A (pH 4.0) (Fig. S10(C and F)†). As expected, these rate constants for the generation of Co^{III}-H from the Co catalyst are consistent with those previously reported by our group of 7.1×10^3 s^{-1} with $TATA^+$ and 0.1 M HA^-/H_2A (pH 4.5)[40] and of 2.6×10^3 s^{-1} with Rubpy and 1.1 M HA^-/H_2A (pH 4.0).[51] Castellano's group has also reported a similar kinetic value of 16×10^3 s^{-1} for the oxidative protonation of a polypyridine cobalt(I) catalyst, to form a Co^{III}-H hydride species, in the presence of Rubpy and 0.3 M HA^-/H_2A (pH 4.0).[33]

Conclusion

In view of increasing the stability of the ruthenium tris-bipyridine photosensitizer (Rubpy) which is the main limitation of such molecular PSs, the water soluble $Na_4[Ru((SO_3Ph)_2-phen)_3]$ analogue (RuSPhphen) was employed. This derivative was tested in combination with the cobalt tetraazamacrocyclic complex $[Co^{III}(CR14)Cl_2]^+$ (Co), one of the most efficient H_2-evolving catalysts in acidic water, and ascorbate (HA^-) as a SD, under visible-light irradiation. Comparative studies under similar experimental conditions with the PS reference Rubpy were also performed. Regardless of the medium, 1.1 M of HA^-/H_2A at pH 4.0 or 0.1 M HA^-/H_2A at pH 4.5 with 1 M acetate buffer, higher photocatalytic performances for H_2 production were obtained with RuSPhphen. In 1.1 M HA^-/H_2A at pH 4.0, the production of H_2 with RuSPhphen is twice at the lower catalyst concentrations of 10 and 5 μM with TON_{Cat} values of up to 2600 and 3170 for RuSPhphen, respectively versus 1380 and 1630 for Rubpy. The H_2 production is always two times higher with RuSPhphen when the PS concentration further decreases to 50 and 25 μM for a catalyst concentration of 10 μM. The higher H_2 production obtained with RuSPhphen can be directly correlated to the higher stability of the photocatalytic system under prolonged irradiation since at catalyst concentrations of 10 and 5 μM, H_2 is produced for more than 10 h with RuSPhphen, while the H_2 production is fully stopped after only 3–4 h for Rubpy. By monitoring the evolution of UV-vis absorption spectra of both PSs during photocatalysis, it was evidenced that RuSPhphen is more stable as a PS than Rubpy, although the initial rate of H_2 production is higher for Rubpy. The stability of both Ru PSs is

further improved when the concentration of the sacrificial electron donor is decreased to 0.1 M. Under such conditions, RuSPhphen still systematically outperforms Rubpy whatever the catalyst concentration, with TONs reaching up to 4770 at 5 μM in the catalyst. This study shows that it is possible to divide by five the quantity of ruthenium PS, while maintaining a high efficiency for H_2 production.

Time-resolved luminescence and nanosecond transient absorption spectroscopy were also employed to study the quenching kinetics of the Ru PS excited state, as well as the associated photocatalytic mechanism, through the detection of key intermediates such as the excited and reduced states of the PSs as well as the reduced form of the catalyst. This photophysical study clearly showed that the first step of the photocatalytic cycle is the reductive quenching of *Ru by HA^-, generating the reduced state $Ru^{\cdot-}$, and that this reductive quenching is faster (k_{red} between 5 and 9×10^7 M^{-1} s^{-1}) for RuSPhphen than for Rubpy (between 1 and 2×10^7 M^{-1} s^{-1}). The RuSPhphen$^{\cdot-}$ species is thus generated very rapidly during photocatalysis, but transient absorption spectroscopy experiments also show that this species disappears very rapidly in the absence of the catalyst (k_{BET} between 1.5 and 2.1×10^{10} M^{-1} s^{-1}), through a back-electron transfer between RuSPhphen$^{\cdot-}$ and the oxidized state of the DS, i.e. $HA^{\cdot}$ or DHA. This rapid charge recombination could contribute to the higher stability of RuSPhphen during photocatalysis, compared to Rubpy, that exhibits a much slower back electron transfer (between 3.5 and 7.4×10^9 M^{-1} s^{-1}). Transient absorption spectroscopy also shows that the reduction of the Co^{II} catalyst to Co^I is just as fast and thermodynamically favorable by RuSPhphen$^{\cdot-}$ (k_{ET} between 2.0 and 3.3×10^9 M^{-1} s^{-1} and ΔG° of -0.46 eV) as by Rubpy$^{\cdot-}$ (k_{ET} of 1.4×10^9 M^{-1} s^{-1} and ΔG° of -0.65 eV). This tends to show that the RuSPhphen PS, in addition to a greater stability, presents a similar reducing power to Rubpy, which should allow it to photo-trigger the activation of a wide panel of molecular catalysts for the reduction of protons to H_2 and also for the reduction of CO_2. Finally, the steric hindrance and rigidity of the SPhphen ligand and the possible delocalization of the radical anion on the conjugated and extended ligand in the reduced state RuSPhphen$^{\cdot-}$, which would then be less prone to losing a ligand in an acidic aqueous medium, could also contribute to the greater stability of RuSPhphen over Rubpy. DFT calculations are underway to evaluate the delocalization of the radical ion on the bpy and SPhphen bidentate ligands in view of rationalizing the difference in stability observed for the two PSs.

Author contributions

The manuscript was written through contributions of all authors. All authors have given approval to the final version of the manuscript.

Conflicts of interest

There are no conflicts to declare.

Acknowledgements

References

1 K. Kalyanasundaram, *Coord. Chem. Rev.*, 1982, **46**, 159–244.

2 A. Juris, V. Balzani, F. Barigelletti, S. Campagna, P. Belser and A. Von Zelewsky, *Coord. Chem. Rev.*, 1988, **84**, 85–277.

3 J. Willkomm, K. L. Orchard, A. Reynal, E. Pastor, J. R. Durrant and E. Reisner, *Chem. Soc. Rev.*, 2016, **45**, 9–23.

4 A. Hagfeldt, G. Boschloo, L. Sun, L. Kloo and H. Pettersson, *Chem. Rev.*, 2010, **110**, 6595–6663.

5 Y.-J. Yuan, Z.-T. Yu, D.-Q. Chen and Z.-G. Zou, *Chem. Soc. Rev.*, 2017, **46**, 603–631.

6 D. Kim and T. S. Teets, *Chem. Phys. Rev.*, 2022, **3**, 021302.

7 R. S. Khnayzer, C. E. McCusker, B. S. Olaiya and F. N. Castellano, *J. Am. Chem. Soc.*, 2013, **135**, 14068–14070.

8 C. K. Prier, D. A. Rankic and D. W. C. MacMillan, *Chem. Rev.*, 2013, **113**, 5322–5363.

9 S. Berardi, S. Drouet, L. Francas, C. Gimbert-Surinach, M. Guttentag, C. Richmond, T. Stoll and A. Llobet, *Chem. Soc. Rev.*, 2014, **43**, 7501–7519.

10 M. H. Shaw, J. Twilton and D. W. C. MacMillan, *J. Org. Chem.*, 2016, **81**, 6898–6926.

11 B. Konig, *Eur. J. Org Chem.*, 2017, 1979–1981, DOI: **10.1002/ejoc.201700420**.

12 Y. Wu, D. Kim and T. S. Teets, *Synlett*, 2021, **33**, 1154–1179.

13 V. Srivastava, P. K. Singh and P. P. Singh, *J. Photochem. Photobiol., C*, 2022, **50**, 100488.

14 Y. Lattach, J. Fortage, A. Deronzier and J. C. Moutet, *ACS Appl. Mater. Interfaces*, 2015, **7**, 4476–4480.

15 K. J. Young, L. A. Martini, R. L. Milot, R. C. Snoeberger, V. S. Batista, C. A. Schmuttenmaer, R. H. Crabtree and G. W. Brudvig, *Coord. Chem. Rev.*, 2012, **256**, 2503–2520.

16 S. Fukuzumi, J. Jung, Y. Yamada, T. Kojima and W. Nam, *Chem.– Asian J.*, 2016, **11**, 1138–1150.

17 S. Ye, C. Ding, M. Liu, A. Wang, Q. Huang and C. Li, *Adv. Mater.*, 2019, **31**, 1902069.

18 M.-N. Collomb, D. V. Morales, C. N. Astudillo, B. Dautreppe and J. Fortage, *Sustainable Energy Fuels*, 2020, **4**, 31–49.

19 N. Queyriaux, R. T. Jane, J. Massin, V. Artero and M. Chavarot-Kerlidou, *Coord. Chem. Rev.*, 2015, **304**, 3–19.

20 T. Stoll, C. E. Castillo, M. Kayanuma, M. Sandroni, C. Daniel, F. Odobel, J. Fortage and M.-N. Collomb, *Coord. Chem. Rev.*, 2015, **304–305**, 20–37.

21 W. T. Eckenhoff, *Coord. Chem. Rev.*, 2018, **373**, 295–316.

22 L. Tong, L. Duan, A. Zhou and R. P. Thummel, *Coord. Chem. Rev.*, 2020, **402**, 213079.

23 R. J. Lim, M. Xie, M. A. Sk, J.-M. Lee, A. Fisher, X. Wang and K. H. Lim, *Catal. Today*, 2014, **233**, 169–180.

24 Y. Yamazaki, H. Takeda and O. Ishitani, *J. Photochem. Photobiol., C*, 2015, **25**, 106–137.

25 J. Bonin, A. Maurin and M. Robert, *Coord. Chem. Rev.*, 2017, **334**, 184–198.

26 N. Elgrishi, M. B. Chambers, X. Wang and M. Fontecave, *Chem. Soc. Rev.*, 2017, **46**, 761–796.

27 M. Stanbury, J.-D. Compain and S. Chardon-Noblat, *Coord. Chem. Rev.*, 2018, **361**, 120–137.

28 K. E. Dalle, J. Warnan, J. J. Leung, B. Reuillard, I. S. Karmel and E. Reisner, *Chem. Rev.*, 2019, **119**, 2752–2875.

29 E. Boutin, L. Merakeb, B. Ma, B. Boudy, M. Wang, J. Bonin, E. Anxolabéhère-Mallart and M. Robert, *Chem. Soc. Rev.*, 2020, **49**, 5772–5809.

30 H. Kumagai, Y. Tamaki and O. Ishitani, *Acc. Chem. Res.*, 2022, **55**, 978–990.

31 J. R. Fisher and D. J. Cole-Hamilton, *J. Chem. Soc., Dalton Trans.*, 1984, 809–813, DOI: **10.1039/dt9840000809**.

32 D. R. Whang, K. Sakai and S. Y. Park, *Angew. Chem., Int. Ed.*, 2013, **52**, 11612–11615.

33 R. S. Khnayzer, V. S. Thoi, M. Nippe, A. E. King, J. W. Jurss, K. A. El Roz, J. R. Long, C. J. Chang and F. N. Castellano, *Energy Environ. Sci.*, 2014, **7**, 1477–1488.

34 T. Stoll, M. Gennari, J. Fortage, C. E. Castillo, M. Rebarz, M. Sliwa, O. Poizat, F. Odobel, A. Deronzier and M.-N. Collomb, *Angew. Chem., Int. Ed.*, 2014, **53**, 1654–1658.

35 M. Vennampalli, G. Liang, L. Katta, C. E. Webster and X. Zhao, *Inorg. Chem.*, 2014, **53**, 10094–10100.

36 C. V. Krishnan, C. Creutz, D. Mahajan, H. A. Schwarz and N. Sutin, *Isr. J. Chem.*, 1982, **22**, 98–106.

37 S. Guo, K.-K. Chen, R. Dong, Z.-M. Zhang, J. Zhao and T.-B. Lu, *ACS Catal.*, 2018, **8**, 8659–8670.

38 W. T. Eckenhoff and R. Eisenberg, *Dalton Trans.*, 2012, **41**, 13004–13021.

39 B. Cecconi, N. Manfredi, T. Montini, P. Fornasiero and A. Abbotto, *Eur. J. Org Chem.*, 2016, **2016**, 5194–5215.

40 R. Gueret, L. Poulard, M. Oshinowo, J. Chauvin, M. Dahmane, G. Dupeyre, P. P. Lainé, J. Fortage and M.-N. Collomb, *ACS Catal.*, 2018, **8**, 3792–3802.

41 D. García-Fresnadillo and G. Orellana, *Helv. Chim. Acta*, 2001, **84**, 2708–2730.

42 R. S. Khnayzer, B. S. Olaiya, K. A. El Roz and F. N. Castellano, *ChemPlusChem*, 2016, **81**, 1090–1097.

43 T. A. White, S. L. H. Higgins, S. M. Arachchige and K. J. Brewer, *Angew. Chem., Int. Ed.*, 2011, **50**, 12209–12213.

44 T. A. White, J. D. Knoll, S. M. Arachchige and K. J. Brewer, *Materials*, 2012, **5**, 27–46.

45 G. F. Manbeck and K. J. Brewer, *Coord. Chem. Rev.*, 2013, **257**, 1660–1675.

46 T. A. White, H. E. Mallalieu, J. Wang and K. J. Brewer, *Chem.– Eur. J.*, 2014, **20**, 8265–8268.

47 G. F. Manbeck, T. Canterbury, R. Zhou, S. King, G. Nam and K. J. Brewer, *Inorg. Chem.*, 2015, **54**, 8148–8157.

48 H. M. Rogers, T. A. White, B. N. Stone, S. M. Arachchige and K. J. Brewer, *Inorg. Chem.*, 2015, **54**, 3545–3551.

49 T. R. Canterbury, S. M. Arachchige, K. J. Brewer and R. B. Moore, *Chem. Commun.*, 2016, **52**, 8663–8666.

50 S. Varma, C. E. Castillo, T. Stoll, J. Fortage, A. G. Blackman, F. Molton, A. Deronzier and M.-N. Collomb, *Phys. Chem. Chem. Phys.*, 2013, **15**, 17544–17552.

51 R. Gueret, C. E. Castillo, M. Rebarz, F. Thomas, A.-A. Hargrove, J. Pécaut, M. Sliwa, J. Fortage and M.-N. Collomb, *J. Photochem. Photobiol., B*, 2015, **152**, 82–94.

52 M. Sandroni, R. Gueret, K. D. Wegner, P. Reiss, J. Fortage, D. Aldakov and M. N. Collomb, *Energy Environ. Sci.*, 2018, **11**, 1752–1761.

53 R. Gueret, C. E. Castillo, M. Rebarz, F. Thomas, M. Sliwa, J. Chauvin, B. Dautreppe, J. Pécaut, J. Fortage and M.-N. Collomb, *Inorg. Chem.*, 2019, **58**, 9043–9056.

54 P. Bugnon and R. E. Hester, *Chem. Phys. Lett.*, 1983, **102**, 537–543.

55 W. K. C. Lo, C. E. Castillo, R. Gueret, J. Fortage, M. Rebarz, M. Sliwa, F. Thomas, C. J. McAdam, G. B. Jameson, D. A. McMorran, J. D. Crowley, M.-N. Collomb and A. G. Blackman, *Inorg. Chem.*, 2016, **55**, 4564–4581.

56 C. Bachmann, M. Guttentag, B. Spingler and R. Alberto, *Inorg. Chem.*, 2013, **52**, 6055–6061.

57 M. Guttentag, A. Rodenberg, C. Bachmann, A. Senn, P. Hamm and R. Alberto, *Dalton Trans.*, 2013, **42**, 334–337.

58 E. Deponti, A. Luisa, M. Natali, E. Iengo and F. Scandola, *Dalton Trans.*, 2014, **43**, 16345–16353.

59 M. Natali, A. Luisa, E. Iengo and F. Scandola, *Chem. Commun.*, 2014, **50**, 1842–1844.

60 L. P. Tong, R. F. Zong and R. P. Thummel, *J. Am. Chem. Soc.*, 2014, **136**, 4881–4884.

61 W. M. Singh, T. Baine, S. Kudo, S. Tian, X. A. N. Ma, H. Zhou, N. J. DeYonker, T. C. Pham, J. C. Bollinger, D. L. Baker, B. Yan, C. E. Webster and X. Zhao, *Angew. Chem., Int. Ed.*, 2012, **51**, 5941–5944.

62 T. Stoll, M. Gennari, I. Serrano, J. Fortage, J. Chauvin, F. Odobel, M. Rebarz, O. Poizat, M. Sliwa, A. Deronzier and M.-N. Collomb, *Chem.– Eur. J.*, 2013, **19**, 782–792.

63 C. Costentin, F. Camara, J. Fortage and M.-N. Collomb, *ACS Catal.*, 2022, 6246–6254.

64 E. Amouyal and P. Koffi, *J. Photochem.*, 1985, **29**, 227–242.

65 D. R. Anton and R. H. Crabtree, *Organometallics*, 1983, **2**, 855–859.

66 B. R. Galan, M. L. Reback, A. Jain, A. M. Appel and W. J. Shaw, *Eur. J. Inorg. Chem.*, 2013, **2013**, 5366–5371.

67 G. M. Brown, B. S. Brunschwig, C. Creutz, J. F. Endicott and N. Sutin, *J. Am. Chem. Soc.*, 1979, **101**, 1298–1300.

68 M. Guttentag, A. Rodenberg, R. Kopelent, B. Probst, C. Buchwalder, M. Brandstätter, P. Hamm and R. Alberto, *Eur. J. Inorg. Chem.*, 2012, **2012**, 59–64.

69 C.-B. Li, A. J. Bagnall, D. Sun, J. Rendon, M. Koepf, S. Gambarelli, J.-M. Mouesca, M. Chavarot-Kerlidou and V. Artero, *Sustainable Energy Fuels*, 2022, **6**, 143–149.

70 M. L. A. Hakkennes, M. S. Meijer, J. P. Menzel, A.-C. Goetz, R. Van Duijn, M. A. Siegler, F. Buda and S. Bonnet, *J. Am. Chem. Soc.*, 2023, **145**, 13420–13434.

71 J. R. Lakowicz, *Principles of Fluorescence Spectroscopy*, Springer, New York, NY, 2017.

72 B. Shan, T. Baine, X. A. N. Ma, X. Zhao and R. H. Schmehl, *Inorg. Chem.*, 2013, **52**, 4853–4859.

73 C. Creutz, N. Sutin and B. S. Brunschwig, *J. Am. Chem. Soc.*, 1979, **101**, 1297–1298.

74 X. Zhang, K. Yamauchi and K. Sakai, *ACS Catal.*, 2021, **11**, 10436–10449.

75 K. Kitamoto and K. Sakai, *Chem. Commun.*, 2016, **52**, 1385–1388.

76 C. V. Suneesh, B. Balan, H. Ozawa, Y. Nakamura, T. Katayama, M. Muramatsu, Y. Nagasawa, H. Miyasaka and K. Sakai, *Phys. Chem. Chem. Phys.*, 2014, **16**, 1607–1616.

77 F. Camara, T. Gavaggio, B. Dautreppe, J. Chauvin, J. Pécaut, D. Aldakov, M.-N. Collomb and J. Fortage, *Molecules*, 2022, **27**, 6614.

78 The $\Delta\varepsilon$ value was determined from the difference in absorption at 510 nm between the spectra of **RuSPhphen** at ground and mono-reduced states presented in Fig. 2.

79 W. M. Singh, M. Mirmohades, R. T. Jane, T. A. White, L. Hammarström, A. Thapper, R. Lomoth and S. Ott, *Chem. Commun.*, 2013, **49**, 8638–8640.